ANRCP-1999-19
May 1999

Amarillo National Resource Center for Plutonium

A Higher Education Consortium of The Texas A&M University System, Texas Tech University, and The University of Texas System

Modeling of the Performance of Weapons MOX Fuel In Light Water Reactors

J. Alvis, P. Bellanger, P.G. Medvedev, and K.L. Peddicord
Nuclear Engineering Department
Texas A&M University

G.I. Gellene
Chemistry and Biochemistry Department
Texas Tech University

DISTRIBUTION OF THIS DOCUMENT IS UNLIMITED

Edited by

Angela L. Woods
Technical Editor

MASTER

600 South Tyler • Suite 800 • Amarillo, TX 79101
(806) 376-5533 • Fax: (806) 376-5561
http://www.pu.org

DISCLAIMER

DISCLAIMER

Portions of this document may be illegible in electronic image products. Images are produced from the best available original document.

AMARILLO NATIONAL RESOURCE CENTER FOR PLUTONIUM/
A HIGHER EDUCATION CONSORTIUM

A Report on

Modeling of the Performance of Weapons MOX Fuel in Light Water Reactors

J. Alvis, P. Bellanger, P. G. Medvedev, and K. L. Peddicord
Department of Nuclear Engineering
Texas A&M University
College Station, TX 77843

G. I. Gellene
Department of Chemistry and Biochemistry
Texas Tech University
Lubbock, TX 79409

Submitted for publication to

ANRC Nuclear Program

May 1999

Modeling of the Performance of Weapons Mox Fuel in Light Water Reactors

J. Alvis, P. Bellanger, P. G. Medvedev, and K. L. Peddicord
Department of Nuclear Engineering
Texas A&M University

G. I. Gellene
Department of Chemistry and Biochemistry
Texas Tech University

Abstract

Both the Russian Federation and the United States are pursing mixed uranium-plutonium oxide (MOX) fuel in light water reactors (LWRs) for the disposition of excess plutonium from disassembled nuclear warheads.

Fuel performance models are used which describe the behavior of MOX fuel during irradiation under typical power reactor conditions.

The objective of this project is to perform the analysis of the thermal, mechanical, and chemical behavior of weapons MOX fuel pins under LWR conditions. If fuel performance analysis indicates potential questions, it then becomes imperative to assess the fuel pin design and the proposed operating strategies to reduce the probability of clad failure and the associated release of radioactive fission products into the primary coolant system.

Applying the updated code to anticipated fuel and reactor designs, which would be used for weapons MOX fuel in the United States, and analyzing the performance of the WWER-100 fuel for Russian weapons plutonium disposition are addressed in this report.

The COMETHE code was found to do an excellent job in predicting fuel central temperatures. Also, despite minor predicted differences in thermo-mechanical behavior of MOX and UO_2 fuels, the preliminary estimate indicated that, during normal reactor operations, these deviations remained within limits foreseen by fuel pin design.

TABLE OF CONTENTS

LIST OF TABLES

LIST OF FIGURES

1. INTRODUCTION

1.1 BACKGROUND

Both the Russian Federation and the United States are pursuing mixed uranium-plutonium oxide (MOX) fuel in light water reactors (LWRs) for the disposition of excess plutonium from disassembled nuclear warheads. The Ministry of the Russian Federation for Atomic Energy (MINATOM) has made a policy statement that the weapons plutonium is a national treasure, which will be utilized to recover its energy value (Murgov, 1995). The U.S. Department of Energy, in its Record of Decision (1997), has identified MOX and immobilization with radioactive fission products as the two disposition options. The objective is to achieve the spent fuel standard as identified by the U.S. National Academy of Sciences study (1994) on the disposition of weapons plutonium.

To use MOX in LWRs, a number of technical issues must be considered concerning the performance of MOX under typical power reactor conditions. To do this, fuel performance models are utilized which describe the behavior of the fuel during irradiation.

While MOX has been chosen as a disposition option in both the U.S. and Russia, neither country has recently manufactured this fuel nor irradiated it in existing power reactors. The current experience base resides in Europe and Japan. As a result, little technical capability for the analysis of MOX use in LWRs exists in the United States.

To address this situation, a project started in 1997 with the Amarillo National Resource Center for Plutonium (ANRC) to draw upon the experience in Europe and to contribute to establishing a capability in the U.S. for modeling of the thermal, mechanical and chemical performance of MOX fuel. The project involved an industrial collaboration with Belgonucléaire of Brussels, Belgium, the world's larger producer of MOX fuel. Over the past three decades, Belgonucléaire has developed the COMETHE fuel performance code. This code has the capability to address both UO_2 and MOX. COMETHE has been developed on the basis of extensive irradiation programs over a number of years, which serve to characterize the fundamental processes in the performance of nuclear fuel.

1.2 OBJECTIVES

The objective of this project is to perform the analysis of the thermal, mechanical and chemical behavior of weapons MOX fuel pins under LWR conditions. Fuel performance evaluation is a key component of any fuel qualification program. In this type of analysis, the anticipated behavior of fuel pins is modeled under irradiation conditions. The need for fuel performance evaluation is to characterize how the fuel will respond over the several years that it will reside inside the reactor. These predictions are important in assuring that the fuel pin will reach target burnup without failure. If fuel performance analysis indicates potential questions, it then becomes imperative to assess the fuel pin design and the proposed operating strategies to reduce the probability of clad failure and the associated release of radioactive fission products into the primary coolant system.

1.3 METHODOLOGY

The fuel performance analysis was performed using the COMETHE from the Belgonucléaire Company (BN). COMETHE is generally directed toward European reactor cycles, which until now have tended to be shorter, usually on the order of 12 months, compared to those used in the United States. In addition, the target burnups of fuel in European reactors have been less than in the United States. However, European utilities are moving toward longer reactor cycles of 18 to 24 months in length and higher fuel exposures. This necessitated extending the

1

modeling of the thermal conductivity module for oxide fuel, both UO_2 and MOX, in COMETHE to higher burnups. Under an agreement, which was concluded with Belgonucléaire, the modeling work was performed through a project funded by the ANRC.

The present project consists of three phases. The first is to extend the thermal modeling capability to the burnup ranges typical of U.S. LWR's utilizing experimental data from international irradiation programs, and incorporate new models into the COMETHE code. This phase of the project is covered in Section 2 of this report. The second phase is to apply the updated code to anticipated fuel and reactor designs, which would be used for weapons MOX fuel in the United States. The third phase is to analyze the performance of the WWER-100 fuel for Russian weapons plutonium disposition. The latter two phases are covered in Sections 3, 4, 5, and 6.

2. MODELING OF AN IRRADIATION EXPERIMENT USING COMETHE-4D RELEASE 23 FUEL PERFORMANCE COMPUTER CODE

2.1 PURPOSE AND SCOPE

COMETHE-4D is the vintage of successive versions of COMETHE (COmputer code for the MEchanical and THErmal behavior of fuel rods) developed by Belgonucléaire in 1967 to describe the in-pile performance of integral fuel rods. Two characters (now 4D) identify the code version. It reflects major functional modifications of the code. Transition to 4D included introduction of burn-up dependent fuel thermal conductivity and the introduction of a temperature threshold for fission gas release (FGR). Release numbering is identified by 3 digits (now 023). It is incremented when minor modifications of models are necessary, for correcting coding bugs, or when numerical methods are updated. Transition to version 23 included refinements in the implementation of the temperature threshold and the modification of material properties including thermal conductivity for use at higher burnups.

To provide data for the model assessment, data was used from a MOX fuel irradiation program. This program was initiated to investigate the behavior of mixed uranium-plutonium (MOX) fuel irradiated to high burnups. This was accomplished by obtaining in-pile data on fuel central temperature and fission gas release using four instrumented MOX fuel segments. The fuel segments were prepared from two MOX fuel rods irradiated in a Pressurized Water Reactor (PWR) in Switzerland for five operating cycles. The extent of fission gas release was measured by means of a pressure transducer mounted on each fuel segment. The temperature was measured using a thermocouple positioned in the fuel stack.

The full-length MOX fuel rods were irradiated during five power cycles at moderate power, achieving a peak pellet burnup of up to 50 GWd/tM. Fuel rods designated R1 and R2 were then taken out of the same fuel assembly. These fuel rods were composed of two MIMAS fabrication batches characterized by different fuel grain sizes. This variation in fuel fabrication characteristics allowed for the study of the influence of grain size and plutonium homogeneity on the production and release of fission gas. The instrumented fuel segments also allowed for the verification of changes in fuel thermal conductivity with increasing fuel burnup.

The Institute for Energiteknikk (IFE) re-instrumented and irradiated the four MOX fuel segments refabricated from the two full-size fuel rods, two segments from rod R1 and two from rod R2 (Lunde, 1996). The irradiation was carried out with pairs of the fuel segments in two different periods in a Boiling Water Reactor (BWR):

- from 19/01/96 to 29/01/96 with fuel segments R1-1 and R2-4 referred to in this report as phase 1, and
- from 09/07/96 to 12/08/96 with fuel segments R1-2 and R2-3 referred to in this report as phase 2.

One of the stated objectives of this program was to generate experimental data that could be used for the verification and validation of mathematical models used in computer codes for the prediction of fuel performance. This report documents the use of the fuel performance computer code COMETHE-4D Release 23 to model the behavior of the experimental fuel segments (Hoppe, 1995). The complete analysis of the irradiation performance of the fuel segments included modeling of the full-length fuel rod performance in the PWR plus modeling of the fuel segments base irradiation in the PWR,

consideration of the geometry effects of the re-fabrication of the fuel rod segments, and completion of the irradiation in the BWR. A short description of the base materials and experiment are presented in Section 2.1.1. A description of the modeling methodology is presented in Section 2.2. Results of the computer analysis and comparison to experimental results are presented in Section 2.5 discussions of the results are presented in Section 2.9.

2.1.1 Experiment Description

The two full-length fuel rods used in the experiment were fabricated from the standard production of Belgonucleaire (BN) MOX fuel for the PWR using the MIMAS process. This production run consisted of a master blend of enriched Pu diluted in depleted UO_2 up to an average pellet enrichment of 6%. The main difference between the fuels used in the two rods was the grain size of the UO_2 matrix. The two rods were loaded into a 14x14 full MOX assembly and irradiated during five operating cycles at moderate power levels.

2.1.2 Instrumentation

Two segments from each fuel rod were cut from the same geometric locations on each rod and sent to IFE at Kjeller for refabrication into instrumented fuel segments. A small amount of fuel was removed from the ends of each segment to allow room for instrumentation, the plenum, and welded end plugs. A hole was drilled into the top of the fuel column and a thermocouple was inserted. The centering of the drilling and the position of the thermocouple were verified by neutron radiography. A pressure transducer was welded to the bottom of the fuel segment. This pressure transducer was mainly composed of a magnet fixed to a small bellow. The free volume in the upper and lower plenum was limited to improve the detection of small amounts of fission gas release.

2.1.3 Irradiation

The experiment was composed of two phases. For each phase, the tests were made in parallel on the corresponding segments of both fuel rods. For practical reasons, the experiment was controlled based on the temperature indicated by the central thermocouple instead of the reactor power. This was done because the thermocouple provided instantaneous information while the reactor power was calculated based on the output of vanadium detectors needing a stabilization period of at least ten minutes.

The first phase was short and limited to the detection of a gas burst release. The power history was designed in short power steps corresponding to a temperature increase of approximately 25°C and a duration of 15 minutes. Each power step was preceded by a preconditioning period of one hour and followed by a return to a lower temperature. The short power steps were intended to limit the amount of fission gas release by diffusional processes. The return to the lower power level accelerated the stabilization of the inner pressure by allowing the microcracks in the fuel to open.

The object of the second phase was to investigate the gas diffusion process. The second phase was similar to the first except that the first power steps where maintained for close to three days in order to accumulate gas on the grain boundaries from diffusional processes. Each power step was followed by a decrease to a lower level to allow for pressure stabilization as was done in the first phase.

2.2 MODELING METHODOLOGY

The complete analysis of the experiment included modeling of the irradiation of the full-length fuel rods in the PWR and modeling of the fuel segment irradiations. The total irradiation history of the fuel segments included a period of base irradiation

in the PWR followed with re-fabrication and the completion of the irradiation in the BWR.

2.3 BASE IRRADIATION

The base irradiation involved modeling of the full-length rods and fuel segments in the PWR.

2.3.1 Full Length Rod Irradiation

Input data used for the modeling of the performance of the full-length fuel rods is located in Schleumger et al (1996) and Van der Heyden (1996). Data is included for both the fuel rod definition and reactor conditions. The power histories are represented in Figure 1 (Irradiation Report, 1995). The power histories for the two full-length rods are different due to their positions in the fuel assembly.

The fuel rods were modeled using 12 axial slices. The irradiation creep multiplier was reduced from the default value and the Zircaloy growth multiplier was increased slightly for both rods R1 and R2. These changes were estimated by performing parametric runs and comparing the calculated diametral deformations and axial growths to the measured values. The reduced creep multiplier lessened the amount of irradiation enhanced creep down of the clad. The Zircaloy growth multiplier was increased to account for the observed growth of the fuel rods after the PWR irradiation. These adjustments were also applied to the fuel segment modeling.

2.3.2 Fuel Segment Irradiation

COMETHE allows the user to change certain input variables during the course of the computer run. However, those variables that define the geometry of the fuel pin must be fixed at the start. Since it was necessary to ensure that the fuel irradiation history was identical for the different fuel segments in the two reactors, it was decided to use the refabricated fuel segment geometry for both

the base irradiation in the PWR and the irradiation in the BWR. This allowed for the continuation of the irradiation without changing the segment geometry or having to implement a restart capability.

The segments were modeled using seven axial slices. The first six slices represented the region composed by solid pellets. The seventh slice represented the location of the thermocouple penetration after re-fabrication. The plenum length was adjusted in order to closely predict the segment free volumes as determined in Mertens (1997).

Input data used in the modeling of the performance of the fuel segments in the base irradiation in the PWR are summarized in Schleumger et al (1996) and Van der Heyden (1996). The power histories used for the base irradiation are shown in Figure 2 (Irradiation Report, 1995).

2.4 BWR IRRADIATION

The refabrication of the segments for the BWR irradiation changed some of the input data. The largest impacts aside from the geometry changes were the purging of the fission gas released during the base irradiation, the refilling of the fuel segments with pure helium at a reduced pressure and changes in the reactor conditions. The power histories used for the two phases of the irradiation are shown in Figures 3 and 4 (Mertens, 1997). Since the total duration of the experiment was short, only the data at the beginning and end of each stable period was used to generate the power profiles. There is a slight difference of 2% in the magnitude of the power between the two fuel segments irradiated during phase 1.

It was necessary to use a solid pellet geometry in the region of the thermocouple penetration in order to accurately predict the segment free volume. There was no power generated in the region of the penetration since the fuel material had been drilled out. The radial power profile was therefore input

5

for both the phase 1 and phase 2 irradiations to reflect the absence of fuel material in this location. In this way, both the free volume and the central temperature could be calculated correctly.

2.5 RESULTS

An analysis of the two full-length fuel rods and the four fuel segments was performed using the COMETHE 4D-023 code. The results of the analysis of the full-length rods are presented in Figures 5 and 6 and include the following information:

- peak temperature, peak linear power, inner pressure, and fission gas release as a function of the irradiation time.

The results of the analysis of the completion of the irradiation in the BWR after fuel segment re-fabrication are presented in Figures 7 through 10. The following information is presented in these figures for each of the four fuel segments:

- peak temperature, peak linear power, inner pressure, and fission gas release as a function of the irradiation time.

2.6 RESULTS FROM THE PWR IRRADIATION

The base irradiation involved modeling of the full-length rods and fuel segments in the PWR.

2.6.1 Full Length Rod Irradiation

Results of the analysis of the full-length rods irradiated in the PWR are presented in Figures 5 and 6.

The integral fission gas release calculated for both rods R1 and R2 was underestimated by COMETHE. The rod inner pressure was also under-estimated due to the under-prediction of fission gas release. The change in the free volume during irradiation of the

full-length rods was also slightly underestimated.

The diametral change in the cladding was accurately predicted. The cladding irradiation enhanced creep was slightly reduced in order to reduce the amount of clad creep down. The amount of axial growth of fuel rods was also predicted accurately. However, the fuel column growth for both rod R1 and R2 were slightly under-predicted.

2.6.2 Fuel Segment Irradiation

Previous calculations using COMETHE for the full pin irradiation in the PWR have consistently under-predicted the amount of fission gas released from the fuel. The code calculations for the fuel segments also under-predicts the amount of fission gas released. The integral fission gas release calculated for the segments obtained from rod R1 was approximately 1.0%. The integral fission gas release calculated for the segments obtained from rod R2 was only approximately 0.4%. This is much less than the estimated segment release from either rod R1 or rod R2. Rod inner pressure only reflects the effects of the change in the linear power with time because of the lack of an appreciable amount of gas release.

2.7 RESULTS FROM THE BWR IRRADIATION (PHASE 1)

The results of the irradiation of fuel segments 1 and 4 in the BWR are presented in Figures 7 and 10.

The calculated temperatures for these fuel segments are just slightly under predicted when compared to the measured temperatures. It should be noted that the coefficient used to account for fuel thermal conductivity changes with fuel burnup had to be increased from the default value of 3.5 m°K/W to 4.2 m°K/W. This change was necessary in order to account for the higher than expected measured temperature at the measured power for the phase 1 irradiation.

6

The phase 1 temperature for a given power is higher than the corresponding phase 2 measured temperature for the same measured power even though the reactor coolant conditions would indicate otherwise (phase 1 coolant temperature < phase 2 coolant temperature).

As with the PWR irradiation, the integral fission gas release calculated for the segments were much less than measured. Since there was no appreciable gas release the calculated inner pressure for both segments was also under-predicted during the ramp phase of the irradiation.

Because of the short length of the irradiation period there was no appreciable axial elongation. When comparing the diameter measurements performed before the irradiation in the BWR with measurements after the experiment, it is clear that there is a small increase in the diameter of the segments resulting from the power ramps. COMETHE reproduces the diameter increase in the segments. The diameter increase results from increased pellet-cladding mechanical interaction due to fuel thermal expansion and swelling during the ramps. The gap remains closed for the entire irradiation.

2.8 RESULTS FROM THE BWR IRRADIATION (PHASE 2)

The results of the irradiation of fuel segments 2 and 3 in the BWR are presented in Figures 8 and 9.

The central thermocouple of Segment 3 failed at the beginning of the BWR irradiation. Therefore, only the measured temperatures from Segment 2 could be used in the analysis. Since the operating conditions for each segment are identical, Segment 2 temperatures were used in comparison to Segment 3 results. The calculated temperatures for both fuel segments 2 and 3 agree well with the measured temperatures. The amount of fission gas released calculated by COMETHE

was accurately predicted. However, the total gas release calculated was larger than measured. This resulted in a higher calculated inner pressure, though the calculation predicted the start of release and acceleration of the release accurately.

Because of the short length of the irradiation period there was no appreciable axial elongation. When comparing the diameter measurements performed before the irradiation in the BWR with measurements after the experiment, it is clear that there is a small increase in the diameter of the segments resulting from the power ramps. COMETHE reproduces the diameter increase in the segments. The diameter increase results from increased pellet-cladding mechanical interaction due to fuel thermal expansion and swelling during the ramps. The gap remained closed for the entire irradiation.

2.9 DISCUSSION

This investigation of the fuel performance of the experiment was principally concerned with the analysis of the BWR phase of the irradiation. The instrumentation of the fuel segments allowed for the in-pile collection of data. This data is invaluable for the determination of the physical phenomena that occur during irradiation. The evolution of the central temperature and inner pressure (gas release) was used in comparison to the calculated values from COMETHE to try and understand these phenomena more thoroughly.

2.10 TEMPERATURE

It is apparent from the comparison of the calculated temperature to measured that the central temperature as measured by the thermocouple during phase 2 is predicted with a good degree of accuracy. The small difference in the calculated temperature versus the measured temperature in phase 1 of the BWR irradiation most likely resulted from uncertainty in the measured power. As was

pointed out in Section 2.7, the measured temperatures in phase 1 were higher than the temperatures measured during phase 2 for the same measured power despite the reactor coolant temperature being 15°C cooler.

It is also interesting to note that for the high gas release observed in the phase 2 irradiation, both the calculations and the experimental data showed a plateau in the temperature versus linear power. This resulted from the contamination of the fill gas with released fission gas degrading the gap thermal conductivity. This occurred even though the gap remained closed for the entire BWR irradiation.

2.11 INNER PRESSURE

The under-prediction of fission gas release for the phase 1 irradiation in the BWR resulted in the calculated inner pressure for Segments 1 and 4 being much less than measured during the final power ramps. The initiation of gas release is well predicted but the magnitude of the release is under-estimated.

The inner pressure is slightly over-predicted for both Segments 2 and 3. This over-estimate resulted from higher than measured total gas release. The amount of fission gas release was predicted accurately. The amount of Xe and Kr calculated to be in the segment free volume was just slightly larger than that measured. However, the calculated He release was much larger than that estimated from the experimental results. The higher than measured Helium release led to a total gas inventory much larger than measured resulting in the over-predicted inner pressure.

2.12 FISSION GAS RELEASE

Fission gas release at low temperatures and high burnup is generally underestimated by COMETHE. Both the PWR and BWR irradiations confirm this under-prediction in this regime. For the high temperature case,

the agreement between calculated and measured is much better.

An interesting conclusion of the experiment was the small difference in fission gas release between the large and small grain size segments for the phase 2 irradiation, and the large difference between the large and small grain size segments for phase 1. Segment 4 had an increase in inner pressure (attributed to fission gas release) of approximately 5 bars in 12 hours. This rate of increase was not matched by any of the other segments until much higher temperatures and hold times were reached in the phase 2 irradiation.

This large increase in fission gas release cannot be attributed to diffusional processes alone since the amount of gas released is too large and the temperature hold time short. However, it could have resulted from a burst release of gas atoms that had been previously trapped on the grain boundaries in the fuel. The gas atoms accumulate on the grain boundaries and its vicinity during the base irradiation. The grain boundary serves as a reservoir for the gas atoms. Consequently, the gas atoms that reach the grain boundaries reside as solute atoms and are ready to be released to the free volume via interlinkage of bubbles on the temperature rise during an increase in power. However, this gas can be trapped along the grain boundary and in the micro-cracks in the fuel due to the high stress state in the fuel. A burst release of gas can occur upon the removal of the pressure imposed on the fuel pellet during the power reduction. The power reduction reduces the stress imposed on the fuel, opening the micro-cracks in the fuel and allowing the trapped gas to escape to the open free volume of the fuel pin.

The base irradiation plays a large role in this process. Because of the larger gas release during the base irradiation of Segment 1 (due to higher power and despite the larger grain size), the grain boundaries had already been

purged of most of the trapped gas. The small release of gas from the segment resulted from any remaining amount of gas on the grain boundaries and a small amount of gas diffusion.

During phase 2 irradiation, no burst of fission gas was detected. This could have resulted from the power reduction between the ramps not being sufficient to allow for the opening of the microcracks in the fuel. This combined with the high fuel temperature resulted in any burst release being hidden by diffusional releases. Another competing process that could have hindered the observation of a burst release was the shape of the axial power profile. Because the axial power shape peaked near the top of the segment for the phase 2 irradiation compared to phase 1, the time necessary for the released fission gas to come to equilibrium with the pressure transducer (located at the bottom of the fuel segment) could have masked any type of burst release.

Fission gas release was slightly over-predicted for the phase 2 irradiation. The calculations showed that the grain size did not have much of an influence on the quantity of gas released, though the difference in grain size between rods R1 and R2 was only 5 μm.

2.13 CONCLUSIONS

The irradiation program was initiated in order to investigate the high burnup behavior of MOX fuel including fission gas release. Full-length fuel rods were irradiated in a PWR. Two rods were then removed and refabricated into four fuel segments with instruments to measure the segment inner pressure and the fuel central temperature.

These segments were then irradiated in a BWR. Modeling of the full-length fuel rods and the four segments was performed with COMETHE-4D Release 23 and the results compared to experimental data.

For the irradiation in the BWR, the temperature calculations correspond satisfactorily with the measurements. For phase 2 of the experiment, higher powers and temperatures, the fission gas release was adequately predicted. An over-estimate of the total gas inventory in the segment free volume led to an over-prediction of the inner pressure for Segments 2 and 3. However, for the lower power and temperature conditions associated with phase 1, COMETHE under-predicts fission gas release and the resulting inner pressure. Fission gas release at low temperatures and high burnup is generally underestimated by COMETHE. Both the PWR and BWR irradiations confirm this under-prediction in this regime. The under-prediction is partly attributable to burst release of fission gas as demonstrated in Segment 4. The current fission gas release models are not equipped to deal with a burst release and therefore cannot accurately predict incidents of burst release of fission gas.

In conclusion, COMETHE did an excellent job in predicting the fuel central temperature for all four segments. At high powers and temperatures, the fission gas release was accurately predicted. However, for low power and temperature conditions, the code under-predicts fission gas release. These situations are being investigated to determine what modifications may be needed in the modeling capability.
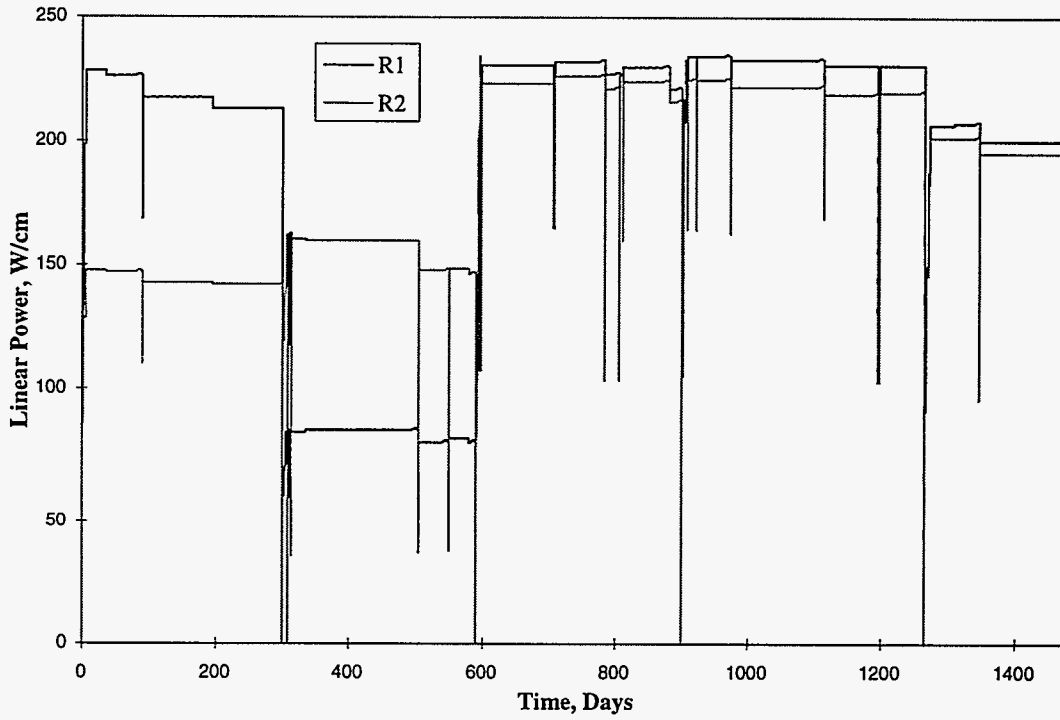
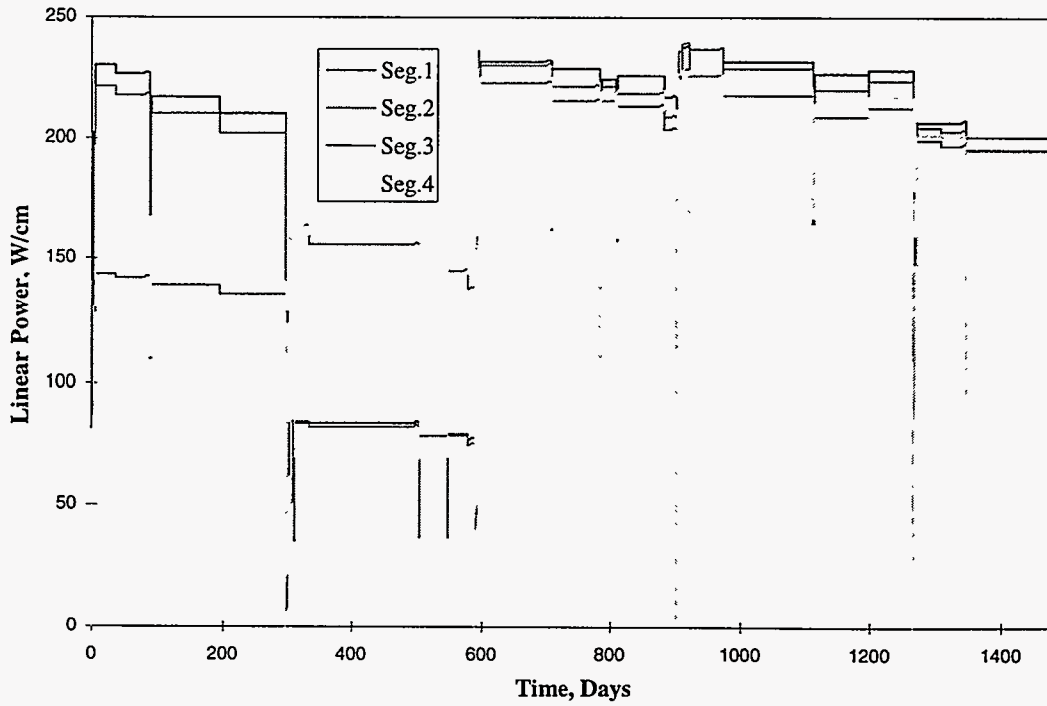**Figure 1:** Power Histories for Full-Length Rods R1 and R2 Irradiation in a PWR

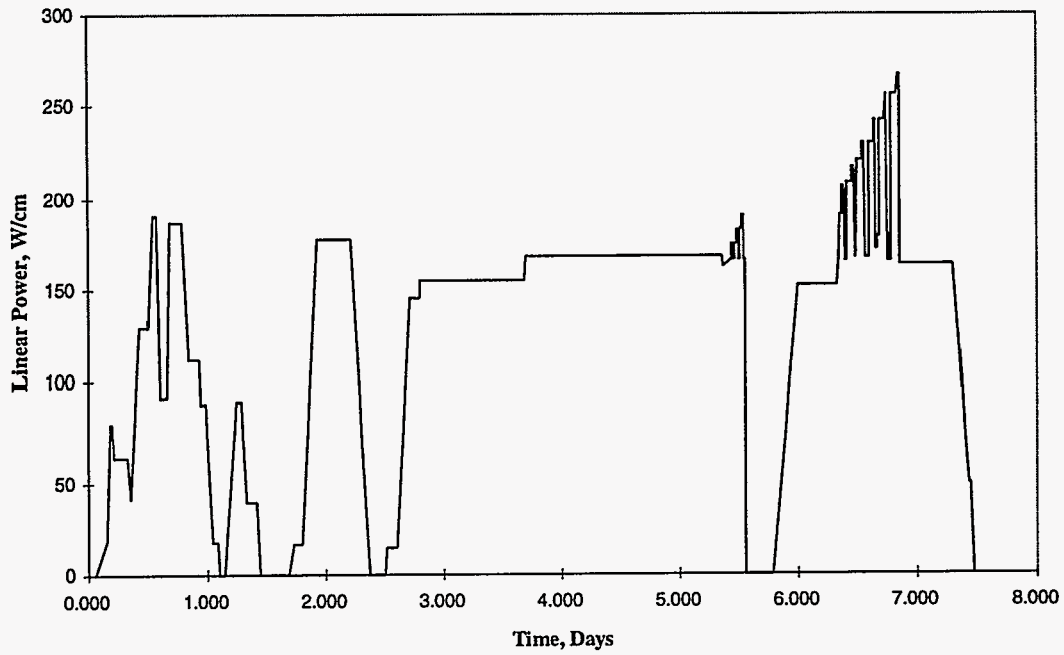**Figure 2:** Power Histories for the Segment Irradiation in a PWR

10

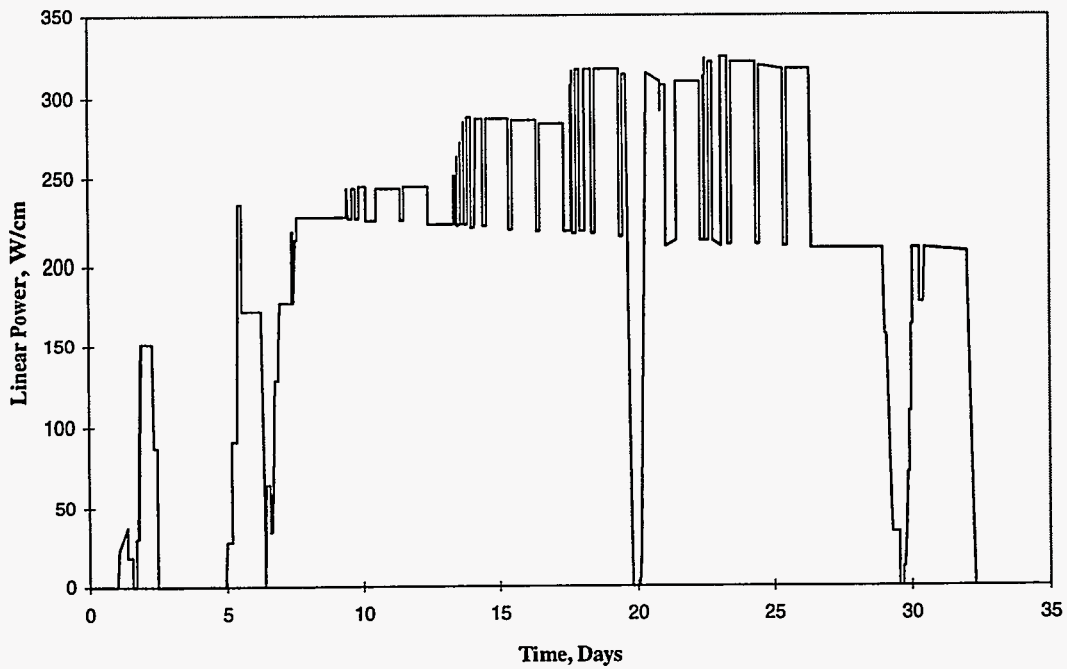**Figure 3:** Power History Used for Phase 1 of the BWR Irradiation

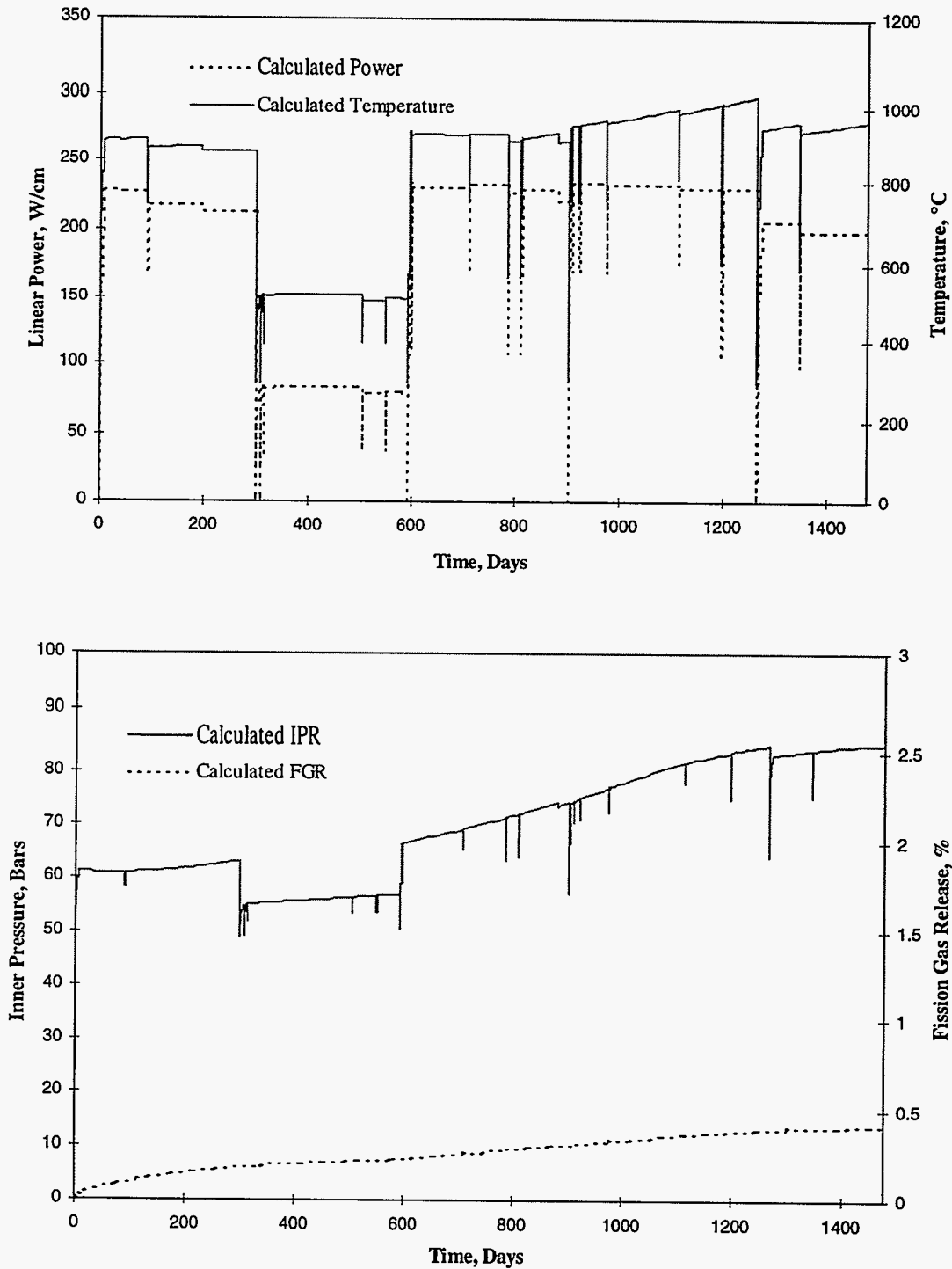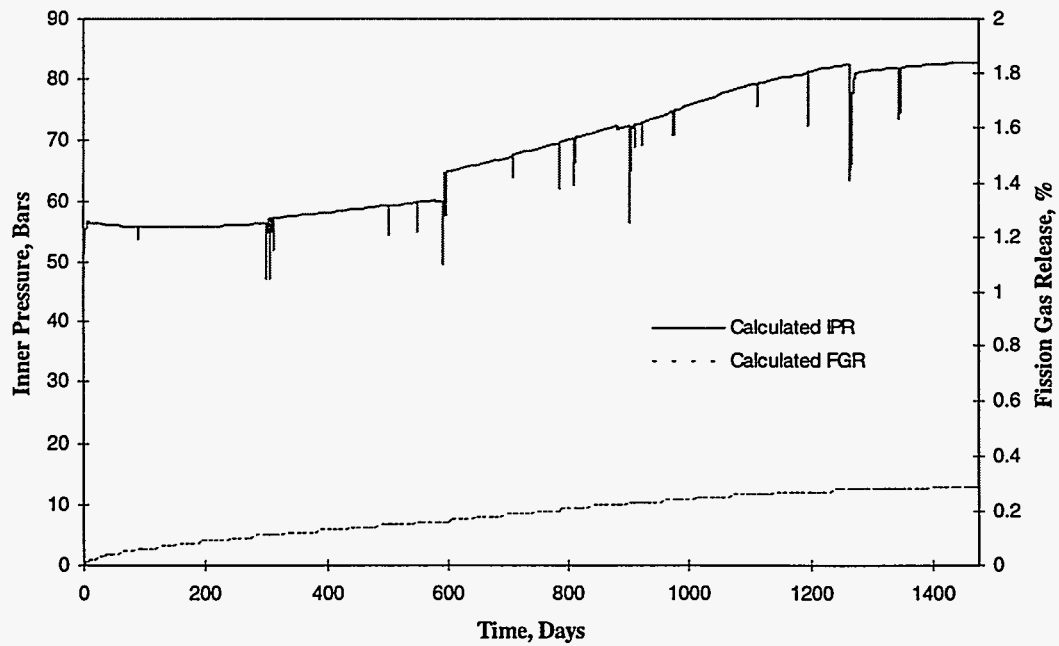**Figure 4:** Power History Used for Phase 2 of the BWR Irradiation

11

Figure 5: Fuel Temperature, Linear Power, Inner Pressure, and Fission Gas Release for the Peak Power Node of Rod R1 During the PWR Irradiation
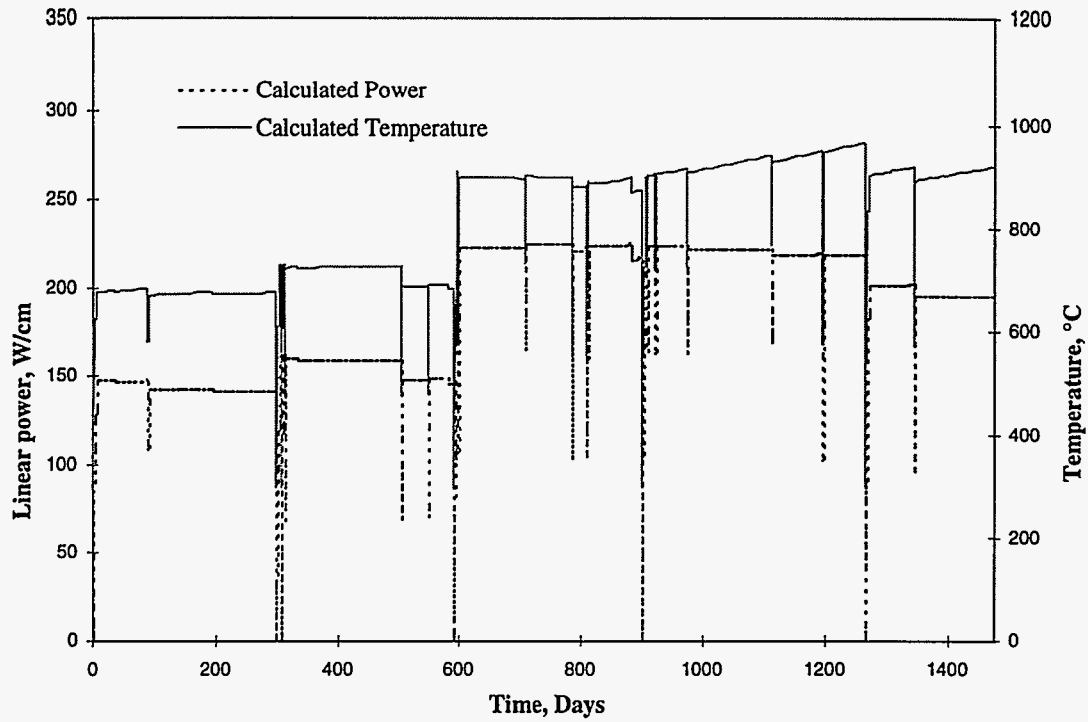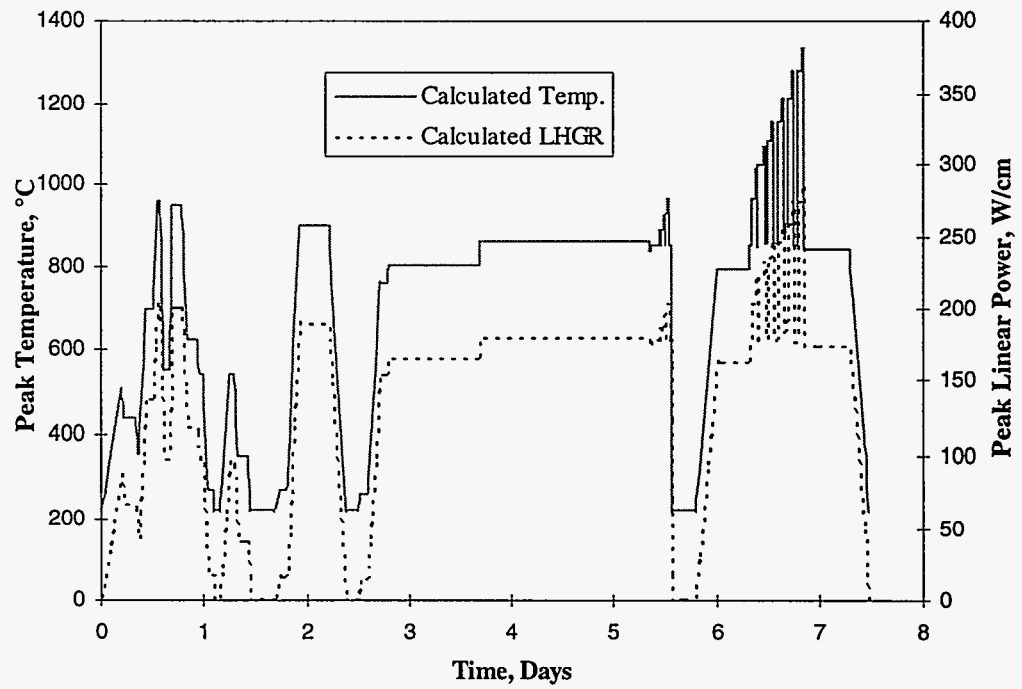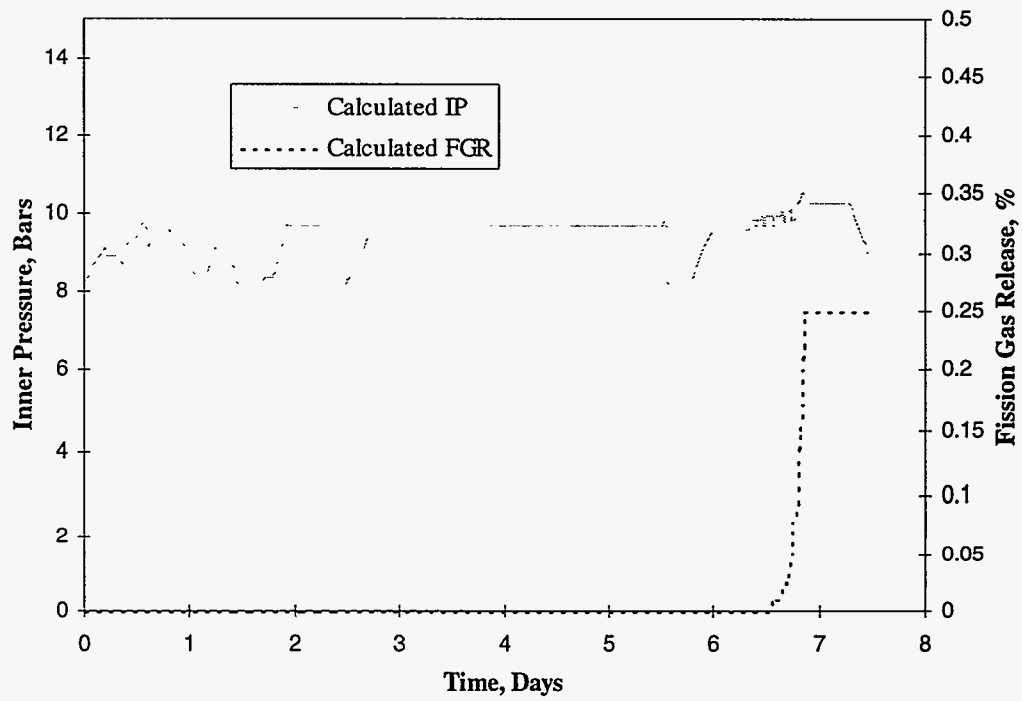
Figure 6: Fuel Temperature, Linear Power, Inner Pressure, and Fission Gas Release
for the Peak Power Node of Rod R2 During the PWR Irradiation

Figure 7: Inner Pressure, Fission Gas Release, Peak Fuel Temperature, and Linear Power Calculated for Segment 1 During the BWR Irradiation
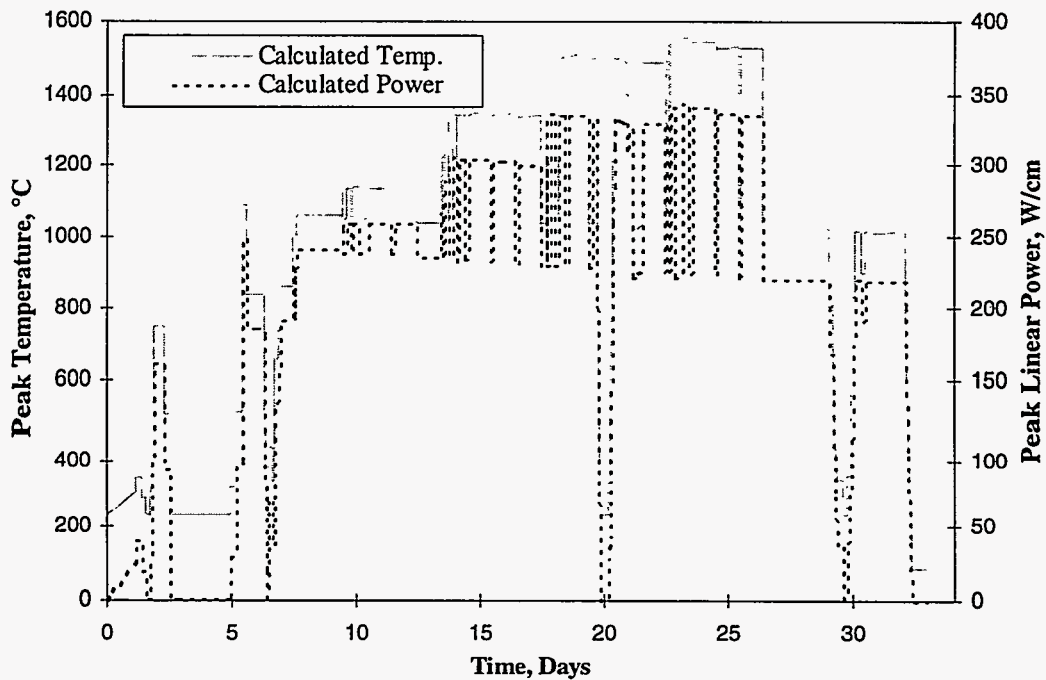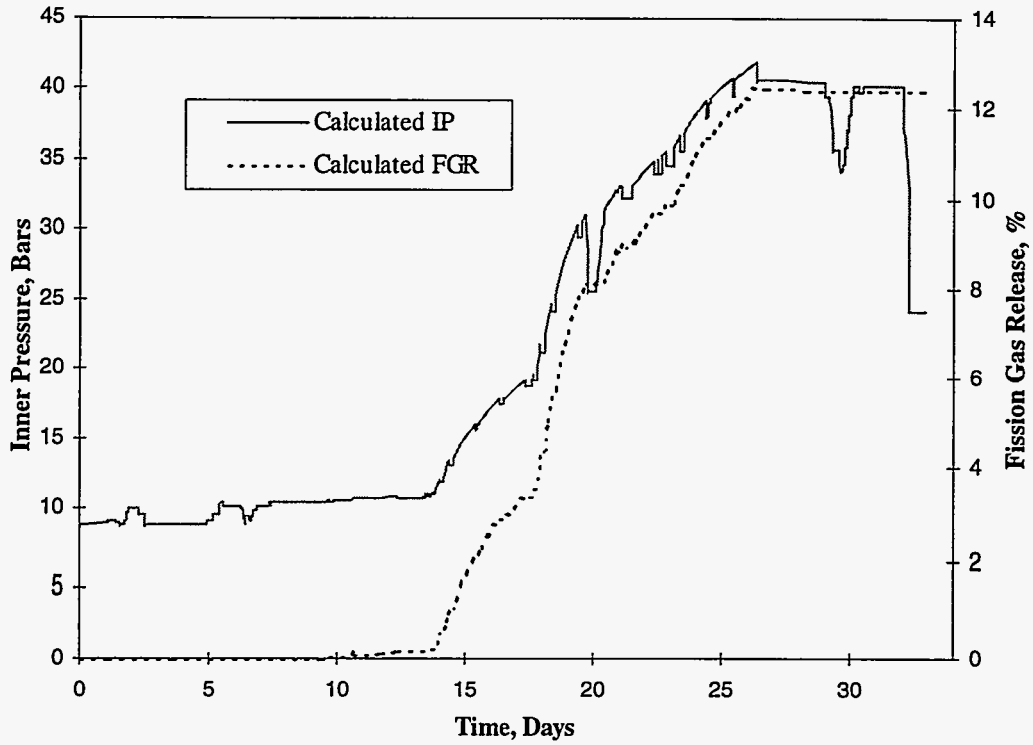
Figure 8: Inner Pressure, Fission Gas Release, Peak Fuel Temperature, and Linear Power Calculated for Segment 2 During the BWR Irradiation
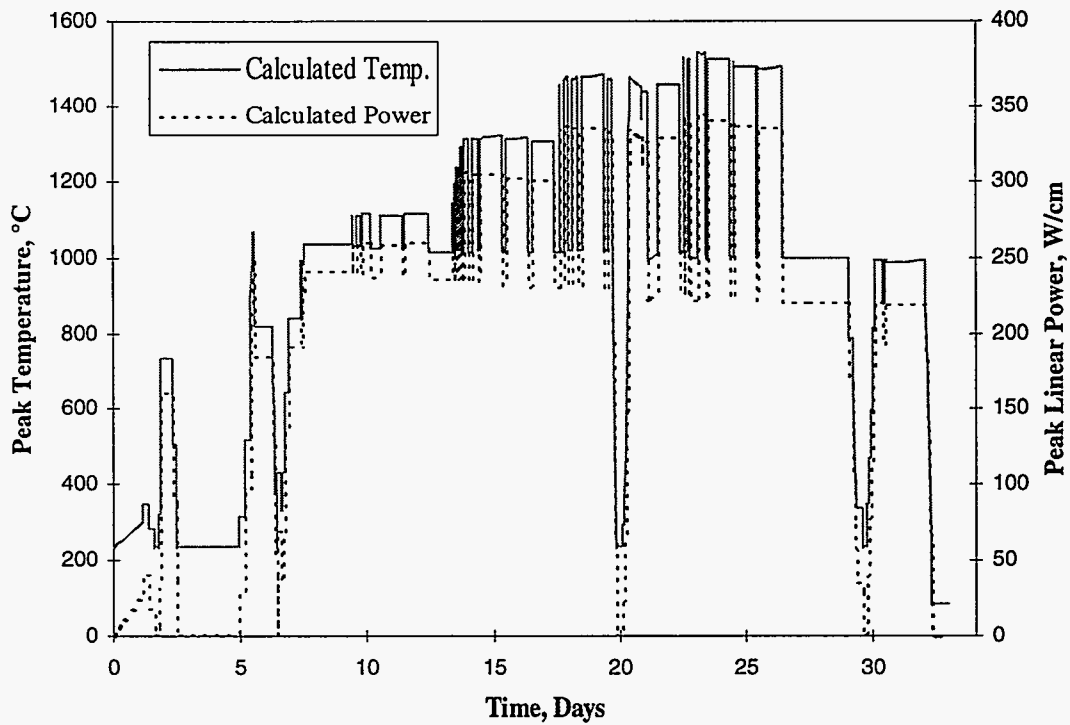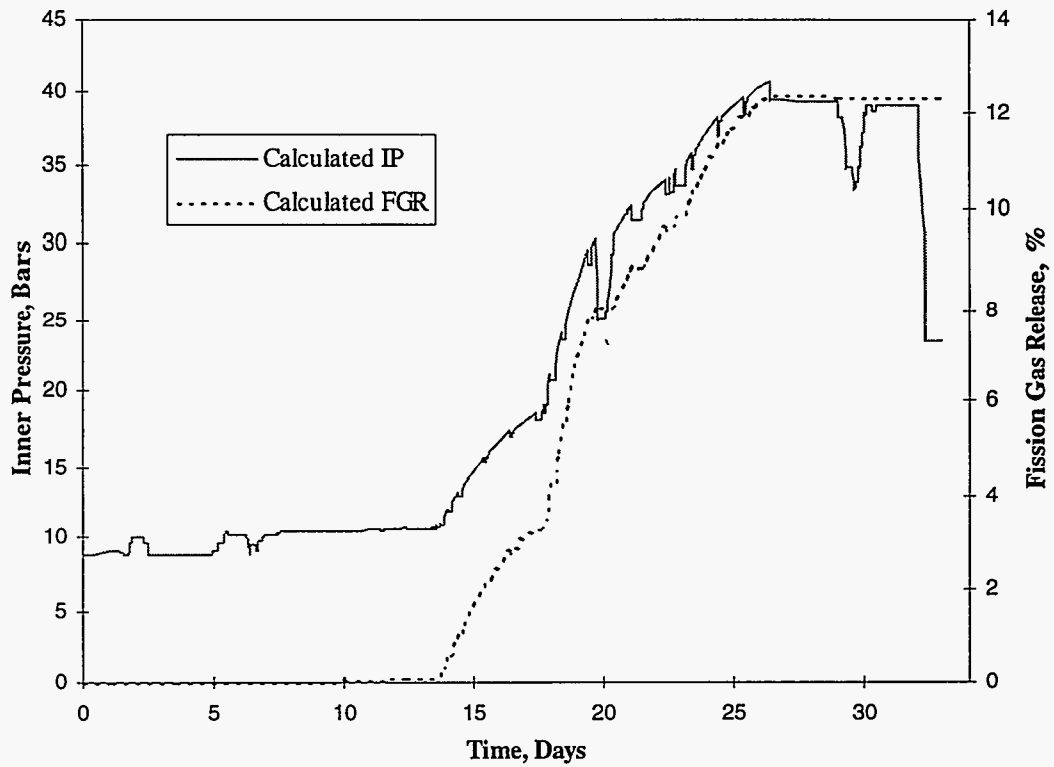
Figure 9: Inner Pressure, Fission Gas Release, Peak Fuel Temperature, and Linear Power Calculated for Segment 3 During the BWR Irradiation
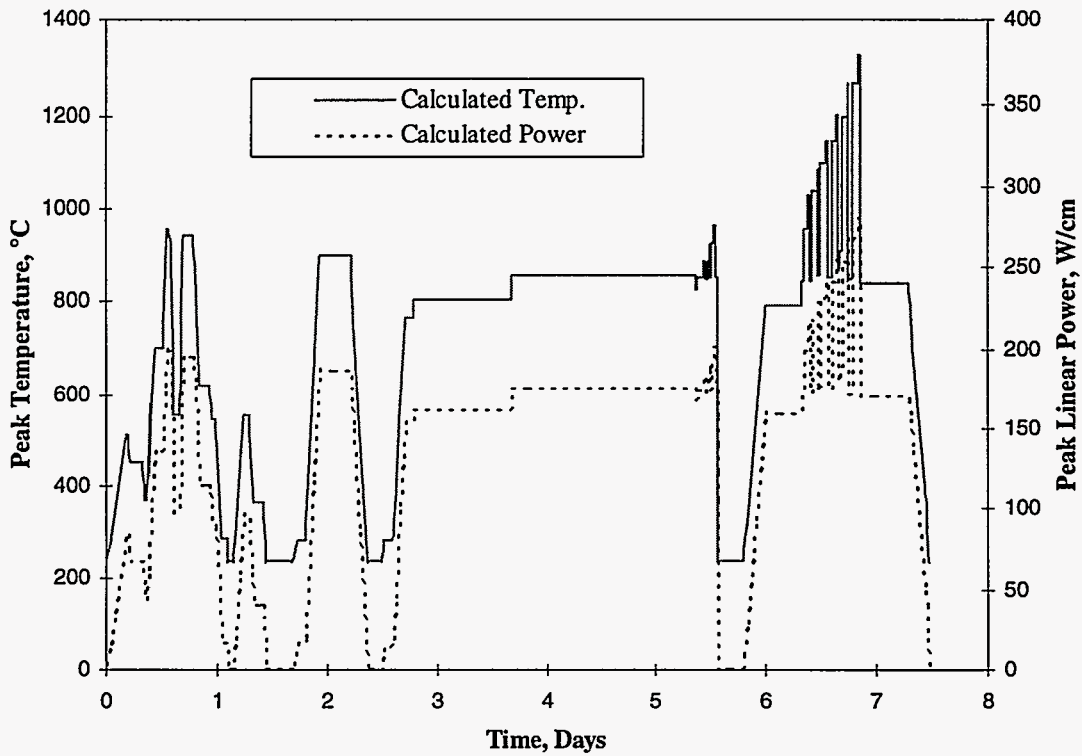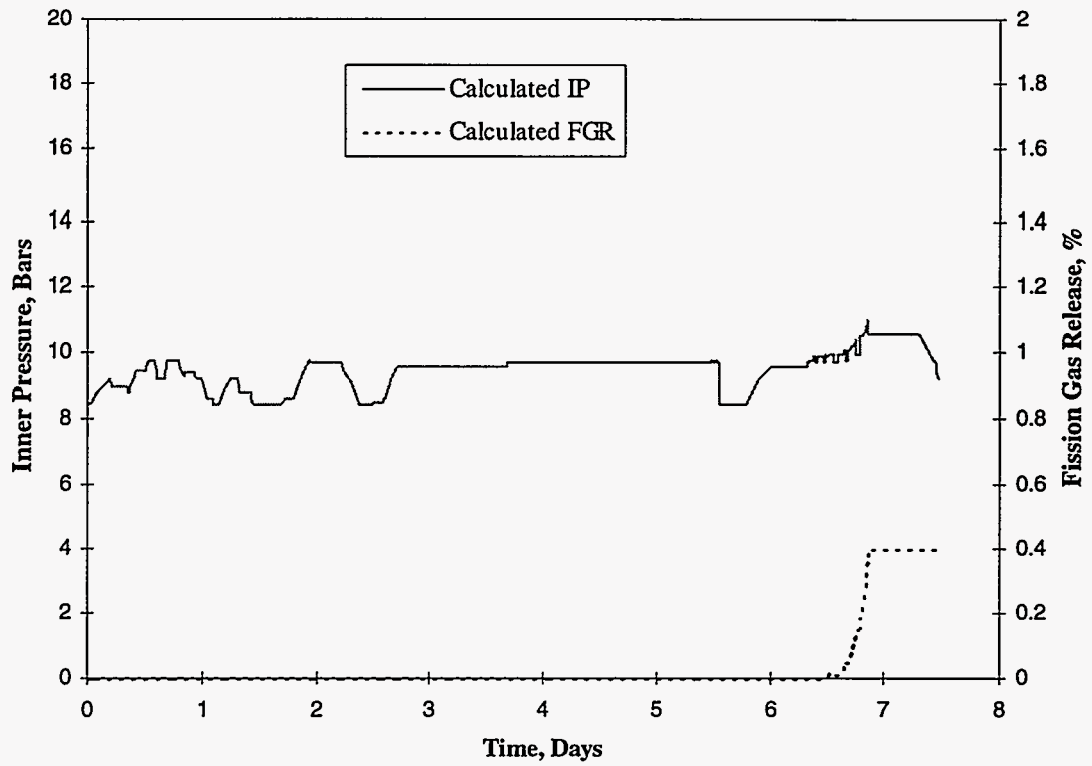
Figure 10: Inner Pressure, Fission Gas Release, Peak Fuel Temperature, and Linear Power Calculated for Segment 4 During the BWR Irradiation

3. EVALUATION OF WEAPONS-GRADE MOX FUEL PERFORMANCE IN LWRs USING COMETHE-4D RELEASE 23 FUEL PERFORMANCE COMPUTER CODE

3.1 PURPOSE AND SCOPE

The purpose of this study is to apply COMETHE (COmputer code for the MEchanical and THErmal behavior of fuel rods) to the designs of the fuel rods and the operation conditions of Light Water Reactors (LWRs) that would be used for disposition of the weapons-grade plutonium in the United States and Russian Federation. These reactor types (PWR, BWR, and WWER) were designed to use uranium oxide fuel. The present study is focused on assessing the difference in thermo-mechanical behavior of the weapons-grade MOX fuel as compared to the conventionally used uranium oxide fuel during normal operational conditions.

3.2 CASES ANALYZED

3.2.1 Fuel Characteristics

Preliminary US-Russian discussions (ORNL Report) indicate that in both countries the weapons-grade MOX fuel will be manufactured using a process similar to the MIMAS (Micronized Master Blend) process adopted by Belgonucléaire and described elsewhere (Deramaix, et al, 1991). In this process the PuO_2 powder is micronized with depleted UO_2 powder to form a master blend with plutonium content in the range of 20 to 30%. This primary blend is than mixed with the depleted UO_2 powder to yield the required plutonium content of 4 to 5 %. The microstructure of the fuel pellet obtained after sintering of the final powder mixture is described as consisting of the plutonium-rich agglomerates dispersed in the UO_2 matrix, and is quantified by the following parameters: plutonium content in plutonium-rich agglomerates, diameter of plutonium-rich

agglomerates, plutonium content of the UO_2 matrix, diameter of the grain of the UO_2 matrix. This is a primary difference in the microstructure of the MOX fuel and conventional UO_2 fuel. The latter usually consists of approximately equisized UO_2 grains. To account for this difference, parameters of the MIMAS fuel, specified above, were incorporated in the input files relevant to the weapons-grade MOX cases.

The composition and the microstructure of the MOX and UO_2 fuels are shown in Table 1 and Table 2, respectively. Table 1 includes parameters characterizing the microstructure of the MIMAS-manufactured MOX fuel such as plutonium content in plutonium-rich agglomerates, diameter of plutonium-rich agglomerates, plutonium content in the UO_2 matrix, and the grain size of the UO_2 matrix. Table 2 has the data relevant to the UO_2 fuel.

3.3 PRESSURIZED WATER REACTOR (PWR)

Four loop Westinghouse PWRs loaded with 17 x 17 fuel assemblies is the most likely candidate for the disposition of weapons-grade plutonium in pressurized water reactors. The relevant parameters to this study are shown in Table 3.

A power history used in the present study was built with respect to the three following requirements. First, a three-batch core management scheme (Nuclear Fuel Cycle) was considered. Therefore, the rod is irradiated three consecutive cycles lasting 18 months each, which is equivalent to 17 GWd/tox. Second, the rod is first loaded at the periphery of the core and is then located closer to the center after each refueling to model an in-out refueling pattern (same reference as before). Finally, the fuel rod is located in a 17x17 assembly, where the average linear heat rate of the rod (Nuclear Power Technology, 1983) is 177 W/cm. The resulting power history is shown in Figure 11a. A time dependent axial power profile

was also considered. Figure 12a shows the axial power profile at the beginning of life. The total irradiation time of the studied rod was 1583 days, which corresponds to a final burnup of 54 GWd/tox.

3.4 BOILING WATER REACTOR (BWR)

Commonwealth Edison, Inc. expressed interest to participate in the plutonium disposition mission. This company intends to utilize weapons-grade MOX fuel in its General Electric BWRs. Currently, there is no information available on the type of assembly to be used for this purpose. In this study, 8x8 assemblies had been selected because they represent the worse rod irradiation conditions in terms of linear heat generation rates, as compared to 9x9 or even the recent 10x10 GE assemblies. The main characteristics can be found in Table 3.

A power history for the BWR case was built similar to the PWR case. However, higher linear heat rates are necessary for the BWR case (Nuclear Power Technology, 1983) to account for the smaller number of fuel rods in the core. Moreover, the irradiation time has to be longer in the BWR because a greater mass of fuel is initially contained in the pins. This requirement was necessary to reach high burnup. The resulting power history shown in Figure 11b led to an irradiation time of 1900 days. The discharge burnup was 42 GWd/t. Figure 12b shows the axial power profile at the beginning of life.

3.5 WWER

WWER -1000 has been selected as an option for the plutonium disposition mission in Russian Federation. The design parameters of the WWER-1000 fuel pins and the reactor itself necessary for the present study were acquired from the International Atomic Energy Agency Technical Report (1996) on the design and performance of the WWER fuel. The set of data reflecting fuel pin design parameters is shown in Table 3. Unlike most other fuels, the WWER fuel pellets feature a central void that has a diameter of 2.4 mm, for the case of WWER-1000. The purpose of the central void is to reduce the fuel centerline temperature during operation, and to provide extra free volume in the pin to accommodate fission gas release. Note, that fuel pin designs, and irradiation histories were identical for the MOX and UO_2 cases studied.

An irradiation history for a WWER-1000 reactor, found in an open source (Shcheglor, et al, 1993), was utilized in this study. This irradiation history is shown in Figure 11c. The maximum linear heat generation rate of 315 W/cm was reached in the beginning of the first cycle. The linear heat generation rate was sufficiently lower during the consequent cycles. This is due to the refueling pattern characteristic for the WWER-1000 reactors. According to this pattern, fresh fuel is initially loaded in the center of reactor core, and than moved towards the core periphery in the consequent cycles. The duration of the irradiation campaign was 876 effective power days, and the burnup at the end of the assembly life reached the value of 46 GWd/t.

3.6 METHODOLOGY

Computer simulation of the in-pile irradiation of the fuel pins using COMETHE is accomplished by incorporating the fuel pin design data and irradiation conditions into a COMETHE input file. Once executed, COMETHE generates a set of output files that contain the fuel performance characteristics calculated for the specified time steps throughout the life of the reactor core. The present study led to the development of six COMETHE input files to simulate MOX and UO_2 cases for each of the three reactor types (PWR, BWR, and WWER). Fuel pin designs currently utilized in the considered reactors were used for development of the COMETHE input files for both UO_2 and MOX cases, i.e. it was assumed that no fuel pin, reactor

design, or operation conditions changes will be adopted during transition of these reactors from UO_2 to MOX. Detailed description of cases analyzed with the emphasis on the fuel pin designs is shown in Section 4.
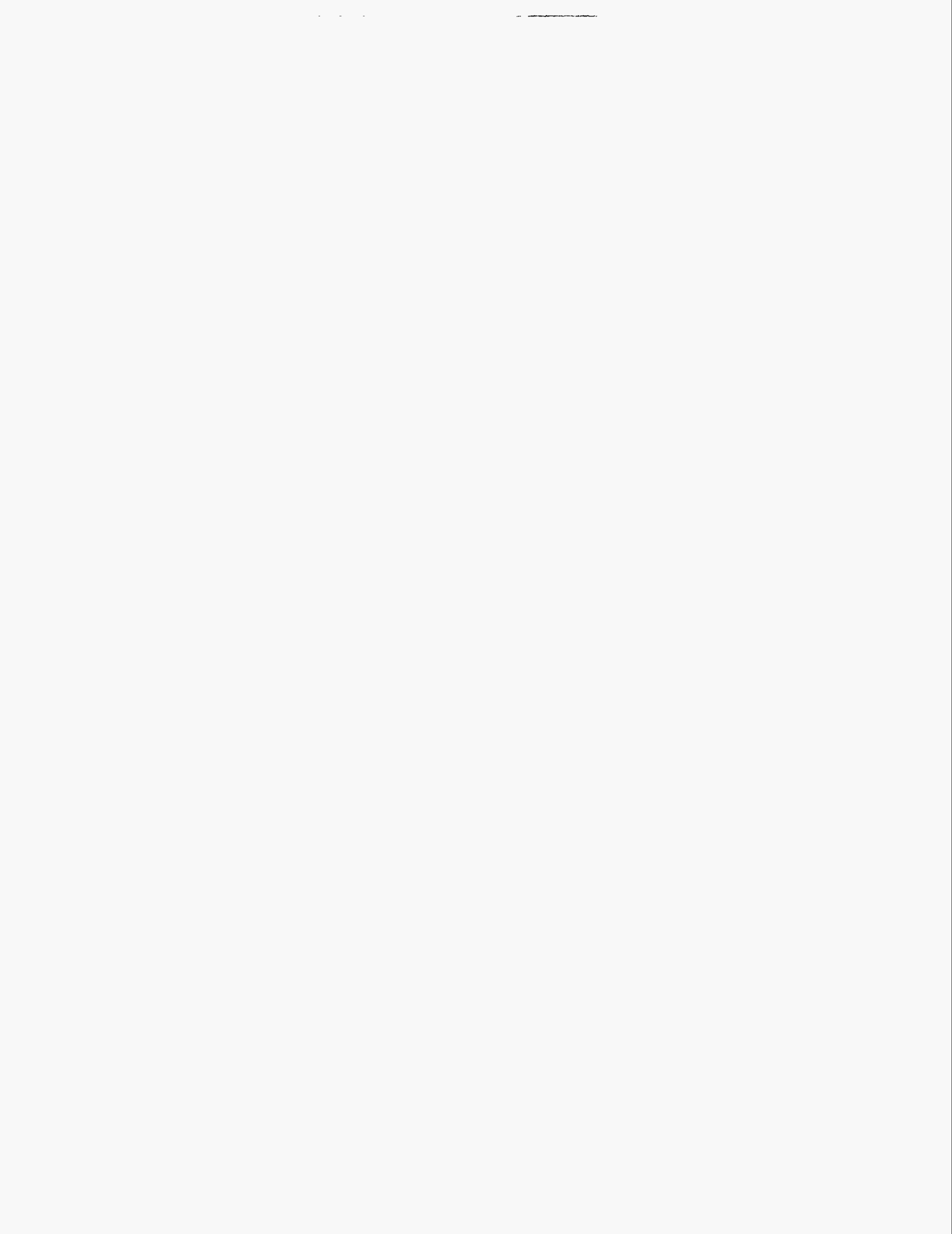
4. RESULTS AND DISCUSSION

4.1 THERMAL BEHAVIOR

Analysis of thermal behavior included evaluation of the fuel temperature, fission gas generation, release, and fuel pin inner pressure.

4.1.1 *Fuel Temperature*

Thermal analysis of the fuel pins revealed that for a given linear heat generation rate, the fuel centerline temperature is slightly higher for the fuel pins loaded with MOX fuel. Figure 13 shows power histories and fuel centerline temperatures for the cases analyzed. A linear increase of the fuel centerline temperature with the increase of the linear heat generation rate of a fuel pin is illustrated in Figure 14.

The difference of the fuel centerline temperatures between UO_2 and MOX fuels is explained by the following phenomena. First, UO_2 fuel has higher thermal conductivity. Second, the fuel-clad gap closes earlier in the fuel pin life for the case of UO_2 (see gap dynamics in Figure 26). Gap closure results in a dramatic improvement of the heat exchange between fuel and coolant, which yields more efficient cooling of the fuel and lower fuel centerline temperature. For the PWR case the gap closure occurs simultaneously for MOX and UO_2, thus only the thermal conductivity is responsible for the temperature difference. For the BWR case, the gap closure is delayed significantly for MOX pins, therefore the temperature difference between UO_2 and MOX is much higher, due to the effects of both gap closure and thermal conductivity. Third, the enrichment for the MOX pellets appears to be higher than the UO_2, which results in a higher peak linear power and higher temperature especially later in the life. Finally, there is a slight difference in the density between the MOX and UO2 used in the cases. This affects the thermal conductivity also.

COMETHE calculations account for the contribution of all these effects.

The trends in thermal behavior of MOX predicted by COMETHE showed agreement with the THERMOX and GRIMOX experiments (Caillot, 1991) performed in France.

4.1.2 *Fission Gas Generation and Release*

Xenon and krypton are the primary fission gases generated in both UO_2 and MOX fuels. Figures 15, 16, 18 and 19 show dynamics of Xe and Kr generation in the fuel and release into the fuel pin free volume. COMETHE predicted that the generation rate of fission gas is approximately the same for UO_2 and MOX. For example, the total amount of fission gas generated during assembly life was 1772 cm^3 (stp) and 1742 cm^3 (stp), respectively, for the WWER-1000 case. However, the fraction of fission gas released into the free volume of the fuel pin was consistently higher for the MOX fuel, and it tends to increase with burnup as shown in Figure 21. Higher fission gas release for MOX fuel was predicted for each of the three reactor designs analyzed in this study.

Higher fission gas release in MOX is explained by higher gas diffusion coefficient in MOX fuel due to the presence of plutonium rich agglomerates, which generate locally large amounts of fission gas. In addition, higher fuel centerline temperature typical for MOX facilitates fission gas release due to the Halden threshold effect, and due to the temperature dependency of the gas diffusion coefficient. Finally, larger amount of helium is generated in MOX fuel due to the radioactive decay of Cm-242, Am-241 and Pu-238, or ternary fission (see Figure 17). Helium has higher diffusion coefficient compared to fission gases, therefore it provides significant contribution to the fission gas release (see Figure 20).

Other experimental and analytical studies (Blanpain, 1994; Doi and Kamate, 1997)

report similar trends of fission gas behavior for experimental and commercial reactors. Also, for the WWER-1000/UO$_2$ case the value of fission gas release predicted by COMETHE agreed with the post-irradiation examination results reported by the IAEA (1996).

4.1.3 Fuel Pin Inner Pressure

Fuel pin inner pressure must remain below reactor coolant pressure throughout the life of the reactor core. Figure 22 proves that for every case analyzed in the present study, the hot fuel pin inner pressure remained significantly less than the coolant pressure. Due to higher fuel temperature and higher fission gas release the fuel pin inner pressure was higher for the MOX cases.

4.2 DIMENSIONAL CHANGES

Dimensional changes that occur in the fuel pin during irradiation include fission induced swelling of the fuel pellet, and creepdown of the clad under the pressure of coolant. These changes result in the decrease and closure of the fuel-clad radial gap. Fuel pin and fuel stack elongation, fuel pellet and clad radius, and fuel-clad gap were chosen as indicators of mechanical performance of the fuel during irradiation. The radii and gap values are reported for the location in the fuel pin that has the highest power density.

4.2.1 Fuel Pin and Fuel Stack Elongation

UO$_2$ and MOX fuels exhibited similar fuel pin and fuel stack elongation during irradiation. Dynamics of the fuel growth are shown in Figure 23. The elongation of the fuel pin did not exceed 1.5 cm, and the elongation of the fuel stack was not more than 5 cm. Values of the fuel pin elongation predicted for the WWER-1000 were in agreement with the experimental data reported by IAEA (Ibid).

4.2.2 Fuel Swelling

Both UO$_2$ and MOX fuels exhibited a tendency to swell under irradiation in a nuclear rector. According to the COMETHE prediction, the UO$_2$ fuel pellet had a higher radius increase due to swelling at the end of irradiation. Dynamics of fuel swelling for the analyzed cases are shown in Figure 24.

4.2.3 Clad Creepdown

Clad creepdown dynamics were found to be similar for the UO$_2$ and MOX fuel pins. Figure 25 illustrates hot clad outer radius as a function of burnup. The outer radius of MOX fuel pins at the end of irradiation was less than that of the UO$_2$ pins. This is explained by less swelling of the MOX fuel as compared to the UO$_2$.

4.2.4 Pellet-Clad Gap

Swelling of the fuel and clad creepdown results in decrease of the pellet-clad gap. The moment when the fuel outer radius becomes equal to the clad inner radius is referred as the gap closure. Since the UO$_2$ fuel swells faster than MOX, the gap closure for the UO$_2$ fuel pins occurs earlier than for the MOX. Pellet-clad gap as a function of burnup is shown in Figure 26. As pointed out earlier, the gap closure leads to the more efficient heat exchange between the fuel pin and coolant, which results in the lower fuel centerline temperature, as was in fact predicted for the UO$_2$ fuel.

4.3 STRESSES IN THE CLADDING

Dimensional changes of the fuel pins induce stresses in the cladding. Clad hoop stress and clad axial stress were evaluated in this study.

4.3.1 Hoop Stress

Fission induced fuel swelling and clad creepdown resulted in a steady increase of the hoop stress in the cladding. Hoop stress in the cladding throughout the assembly life is

shown in Figure 27. As pointed out earlier, swelling is higher for the UO_2 fuel; therefore, higher hoop stresses developed in the fuel pins loaded with the UO_2 fuel.

4.3.2 Axial Stress

As shown earlier, the elongation of the fuel pins during irradiation did not exceed 1.5 cm and no difference was observed between the UO_2 and MOX cases. Fuel pin elongation lead to a positive axial stress in the cladding. For all cases analyzed a rapid increase of the axial stress was predicted in the second half of irradiation campaign for both UO_2 and MOX fuel pins. Dynamics of the axial stress throughout the assembly life are illustrated in Figure 28.

5. PU-239 CONSUMPTION IN THE MOX FUEL

Pu-239 is a major component of the plutonium vector of the weapons grade MOX fuel. Since the primary purpose of weapons-grade MOX utilization in nuclear power plants is the disposition of Pu-239, it was of interest to evaluate the efficiency of such disposition. Figure 29 shows predicted radial distribution of Pu-239 in a MOX fuel pellet at the end of the assembly life. According to this prediction, approximately one-half of the initial amount of Pu-239 is consumed for the considered burnups. Obviously, higher Pu-239 consumption rate can be achieved by increasing burnups.

6. CONCLUSIONS

Comparison of the MOX and UO$_2$ fuel performance in LWRs proposed for disposition of the weapons grade plutonium assessed using COMETHE fuel performance code revealed no significant differences in thermo-mechanical behaviors of these fuels for considered normal operation conditions. The discharge burnups considered in the present study did not exceed 46 GWd/t. Some noticeable differences in the behavior of MOX and UO$_2$ appear in the third cycle, when assembly burnup reaches approximately 30 GWd/t. These differences tend to increase with further increase of burnup.

COMETHE predicted that the MOX fuel pins would operate at the fuel centerline temperature higher than the conventional UO$_2$ pins. This would lead to the increase of the fission gas release, which would also grow with the burnup. COMETHE predicted lower fission induced swelling of the MOX fuel, and, therefore, lower hoop stress in the cladding of the fuel pins loaded with MOX fuel. The calculated consumption efficiency for Pu-239 was equal approximately 50%. Higher burnups may be proposed to increase the consumption of this weapons grade material in the LWRs.

As rule, the thermo-mechanical behavior of MOX and UO$_2$ fuels predicted by COMETHE was similar to that described in the literature. This suggests the validity of the input decks developed for this study.

Despite predicted minor differences in thermo-mechanical behavior of MOX and UO$_2$ fuels, this preliminary estimate indicates that during normal reactor operation these deviations remain within the limits foreseen by the fuel pin design.

Table 1: Weapons-Grade MOX Fuel Composition

Uranium vector (w/o)	U-234	0.002
	U-235	0.200
	U-236	0.001
	U-238	99.797
Plutonium vector (w/o)	Pu-238	0.000
	Pu-239	93.550
	Pu-240	5.900
	Pu-241	0.400
	Am-241	0.05
	Pu-242	0.100
Plutonium enrichment in the fuel (w/o)		5.000
Diameter of Pu agglomerates, μm		100
Pu enrichment in agglomerates (w/o)		0.25
Fraction of Pu in UO_2 matrix (w/o)		0.1

Table 2: UO_2 Fuel Composition

Parameter		Reactor type		
		PWR	BWR	WWER
Uranium vector (w/o)	U-235	3.5	2.5	4.400
	U-238	96.5	97.5	95.600
Grain size of the UO_2 matrix, μm		11.5	11.5	17.5

Table 3: Fuel Rod Characteristics

Parameter		Reactor type		
		PWR	BWR	WWER
Fuel rod length, cm		386.100	410.000	383.300
Active height, cm		366.000	366.000	353.000
Clad outer diameter, mm		9.500	12.500	9.100
Clad inner diameter, mm		8.360	10.780	7.720
Pellet inner diameter, mm		0.000	0.000	2.400
Pellet height, mm		13.500	10.400	11.000
Radial gap, μm		80.000	122.000	130.000
Mean roughness of fuel & clad, μm		5.000	5.000	3.000
Fuel theoretical density, g/cm^3	MOX	10.980	10.980	10.980
	UO$_2$	10.960	10.960	10.950
Total porosity	MOX	0.040	0.040	0.0237
	UO$_2$	0.040	0.040	0.0255
Open porosity		0.004	0.002	0.010
Upper plenum length, cm		17.800	41.700	25.000
Free volume	Upper plenum free volume, cm^3	8.700	37.280	11.720
	Gap, cm^3	7.620	14.950	6.900
	Chamfer, cm^3	0.540	0.910	0.990
	Open porosity, cm^3	0.160	0.260	0.840
	Central hole, cm^3	0.000	0.000	17.340
	Total, cm^3	19.340	57.230	37.800
Constant flow inlet coolant temperature, $^\circ$C		286.000	278.000	289.000
Outlet coolant temperature, $^\circ$C		324.000	288.000	320.000
Lattice pitch, mm		12.6 (Square)	16.2 (Square)	12.75 (Triangular)
Coolant pressure, MPa		15.500	7.030	16.000
Helium pressure, MPa		2.000	2.000	2.500

31
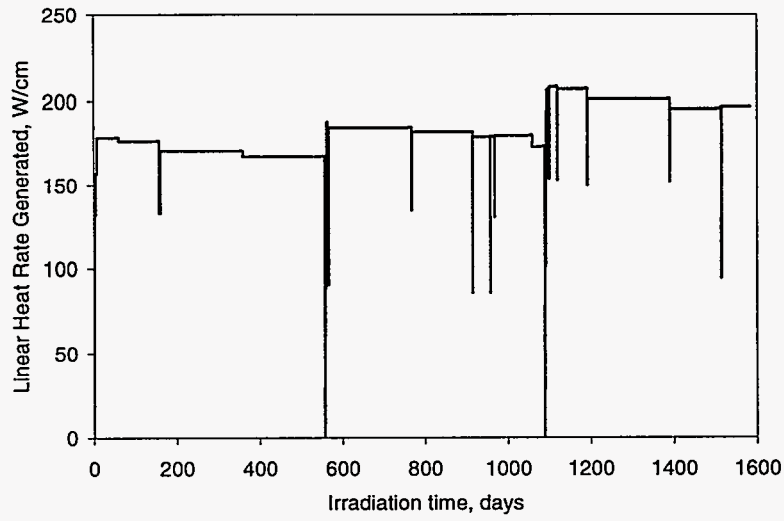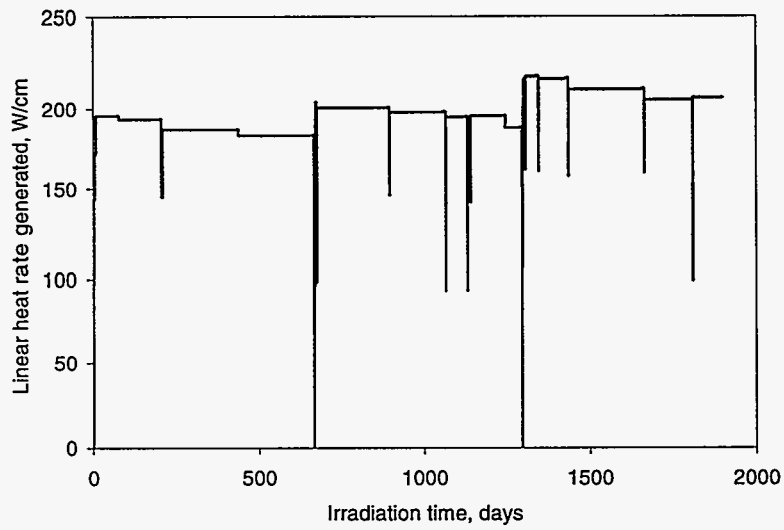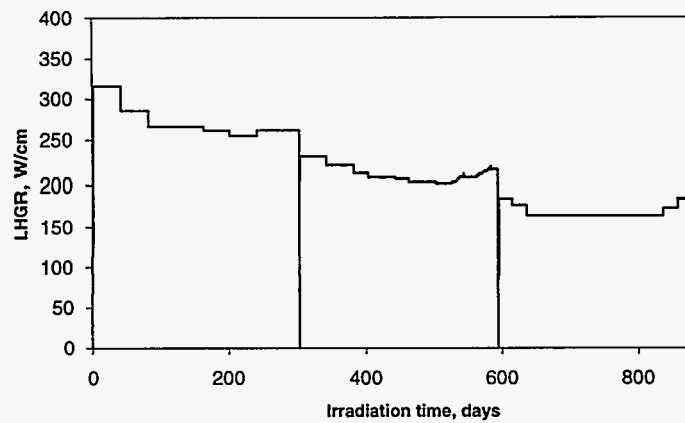
(a) PWR

(b) BWR

(c) WWER

Figure 11: Power Histories for Cases Analyzed

32
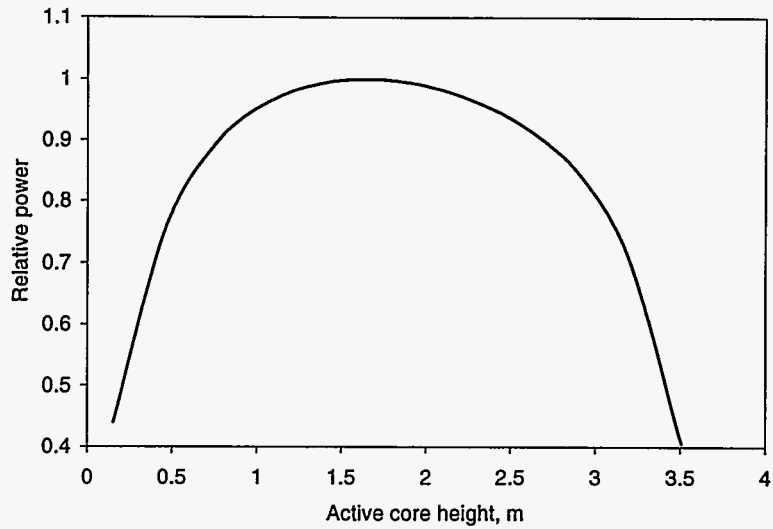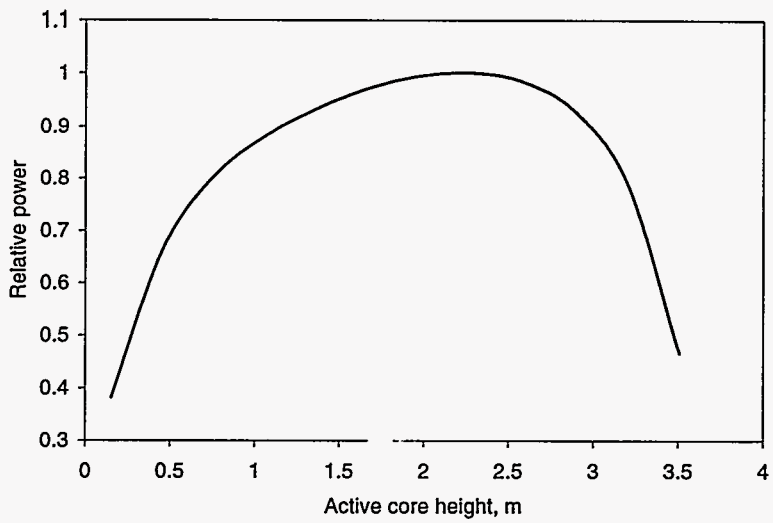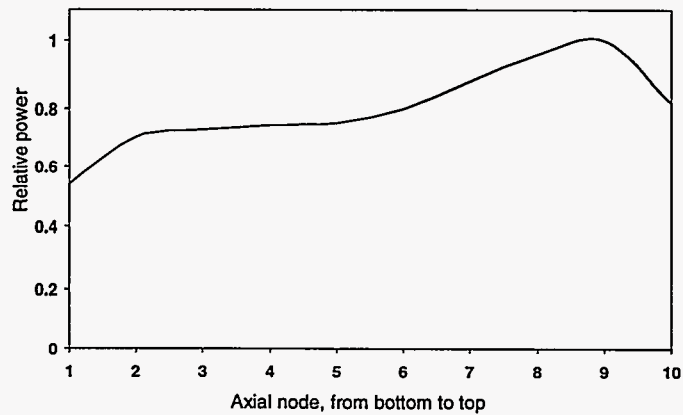
(a) PWR

(b) BWR

(c) WWER

Figure 12: Axial Power Profile at the Beginning of Life

(a) PWR
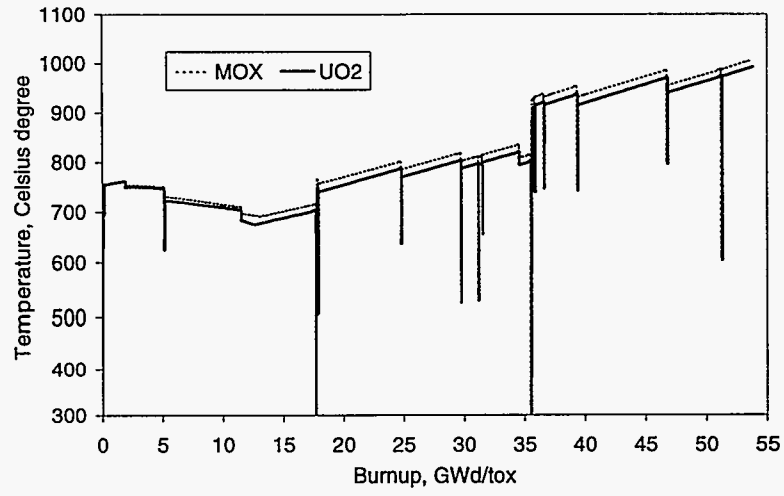
(b) BWR
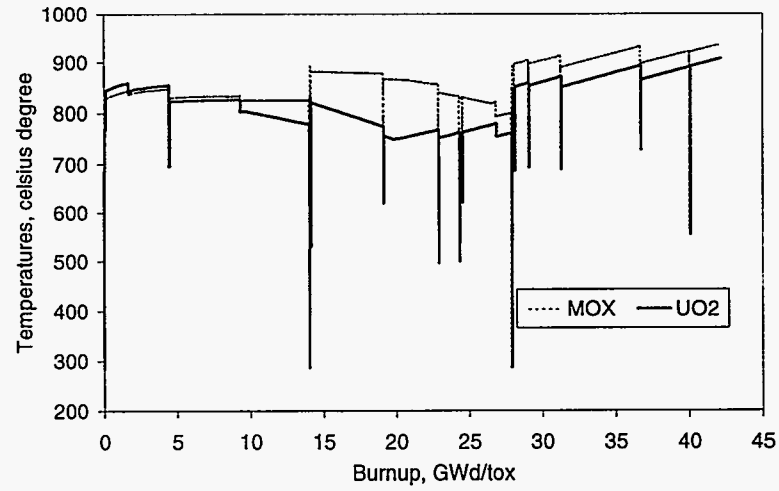
(c) WWER
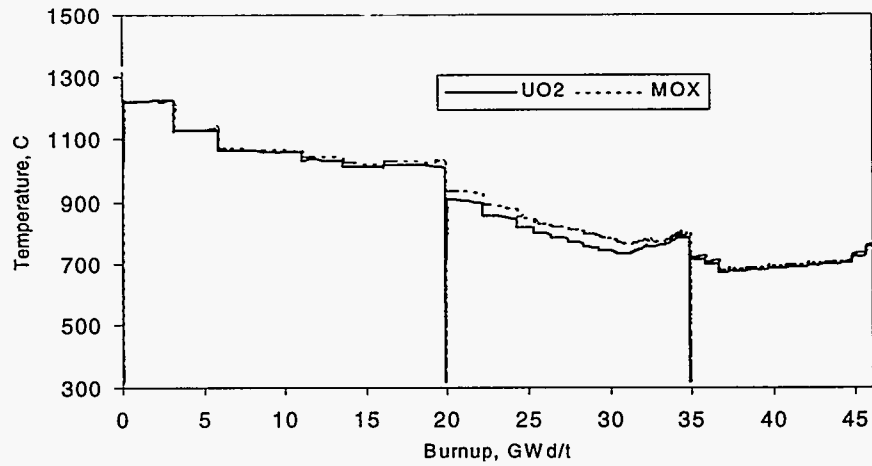
Figure 13: Fuel Centerline Temperature

(a) PWR
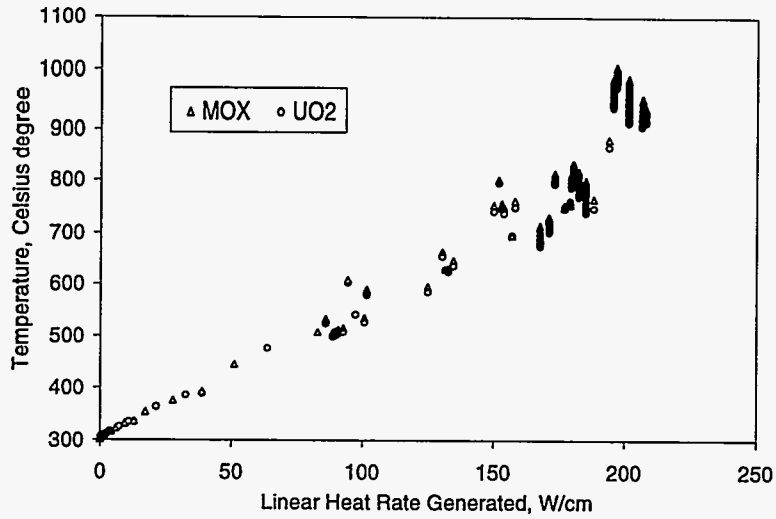
(b) BWR
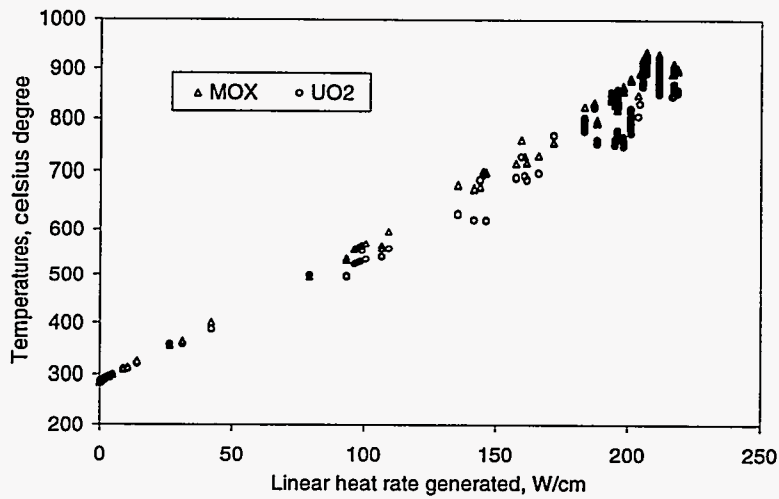
(c) WWER
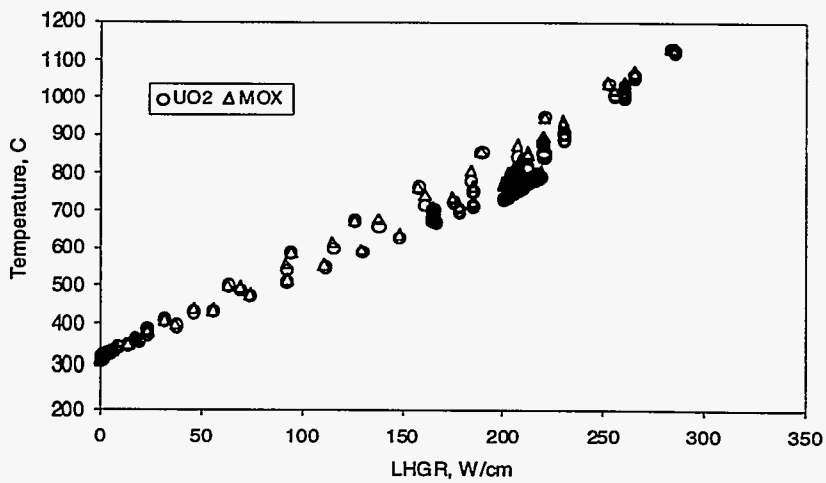
Figure 14: Fuel Centerline Temperature as a Function of Linear Heat Generation Rate

(a) PWR
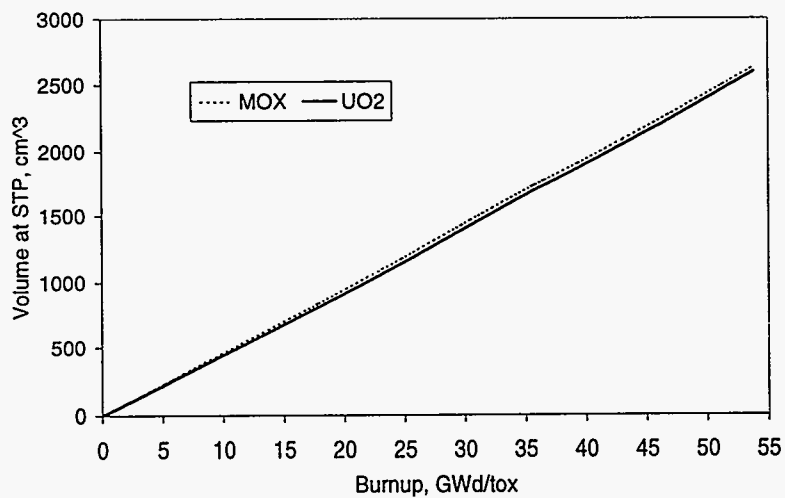
(b) BWR
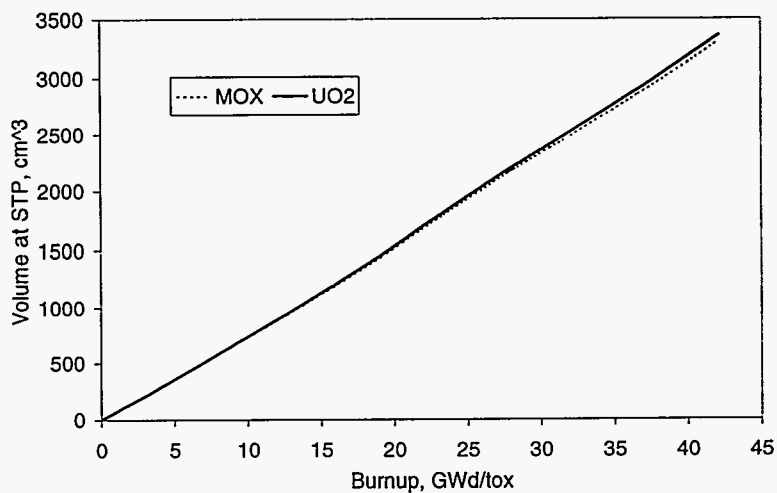
(c) WWER
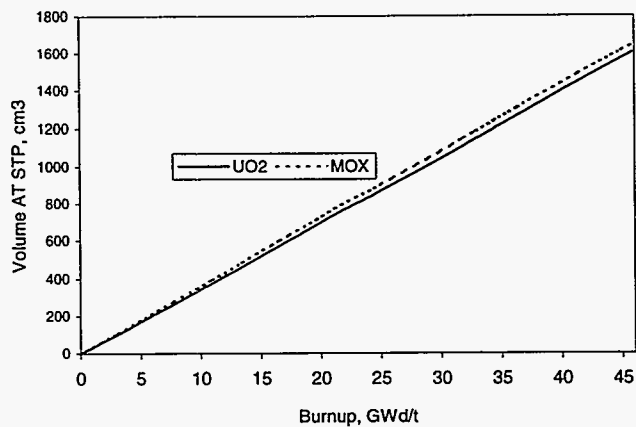
Figure 15: Xe Generation in the Fuel
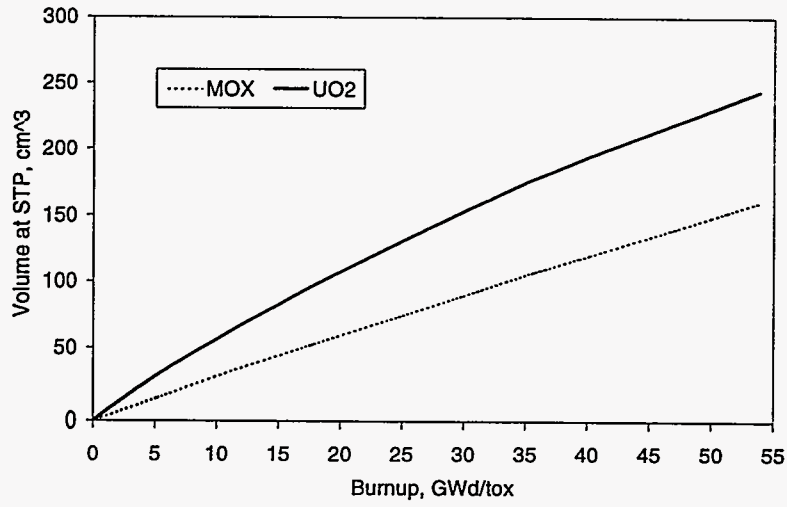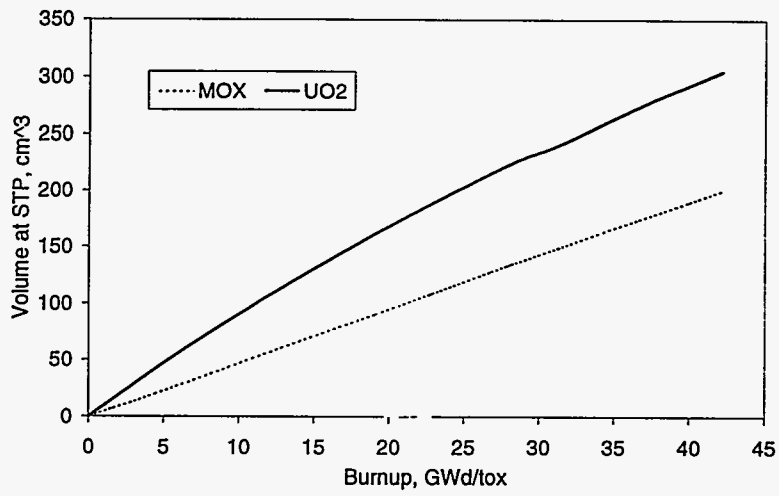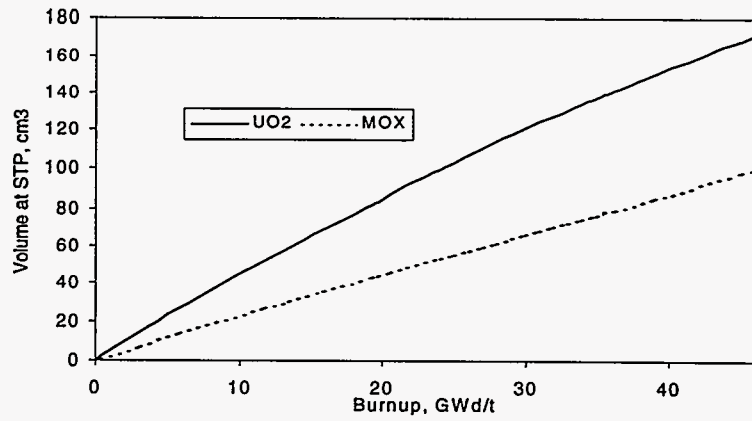
(a) PWR

(b) BWR

(c) WWER

Figure 16: Kr Generation in the Fuel

37
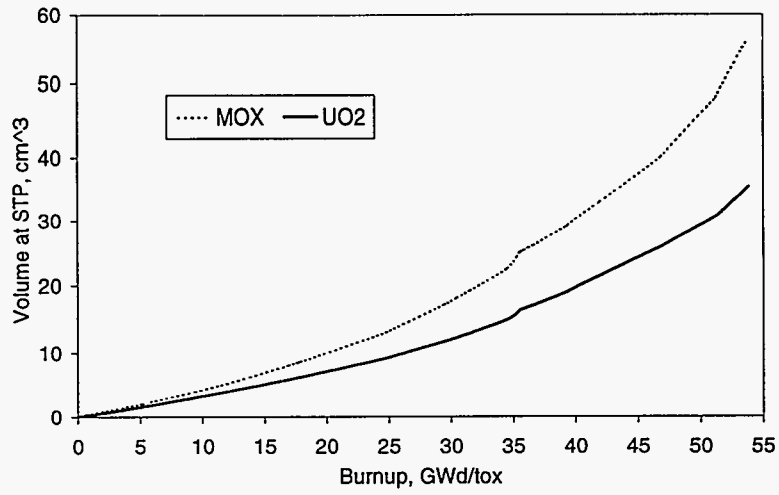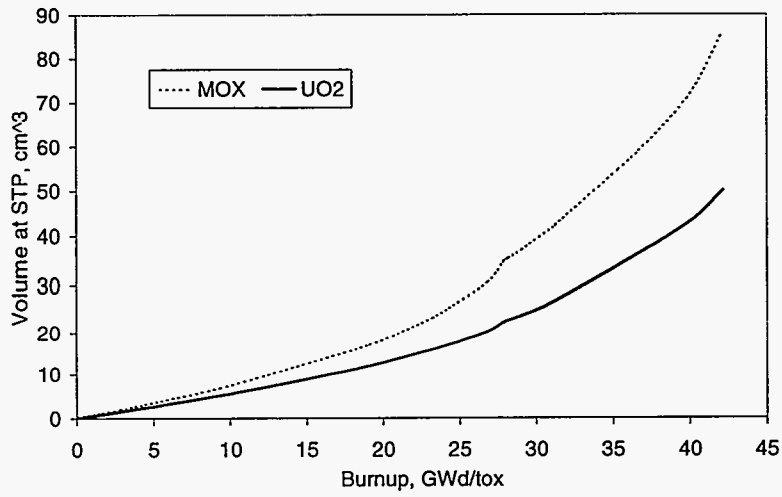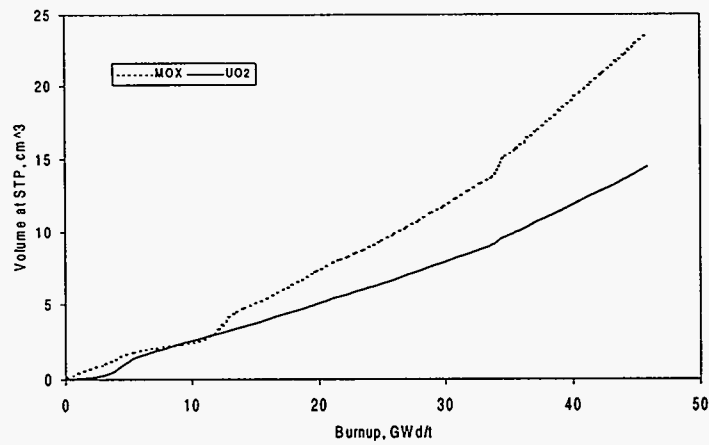
(a) PWR

(b) BWR

(c) WWER

Figure 17: He Generation in the Fuel
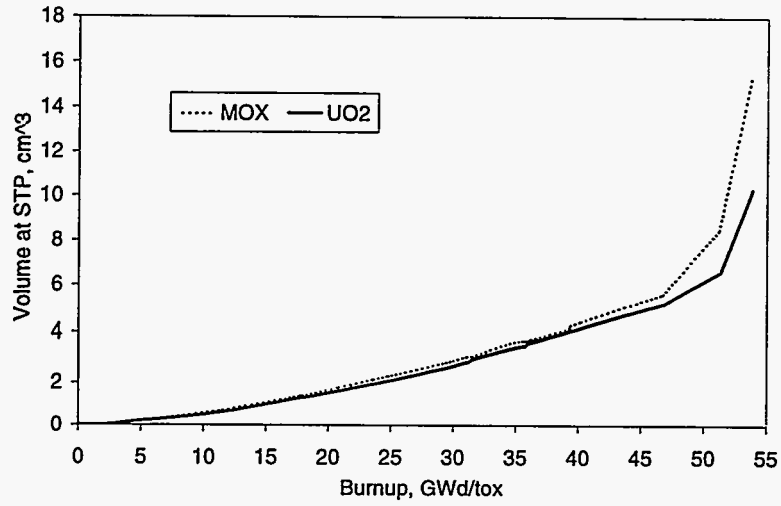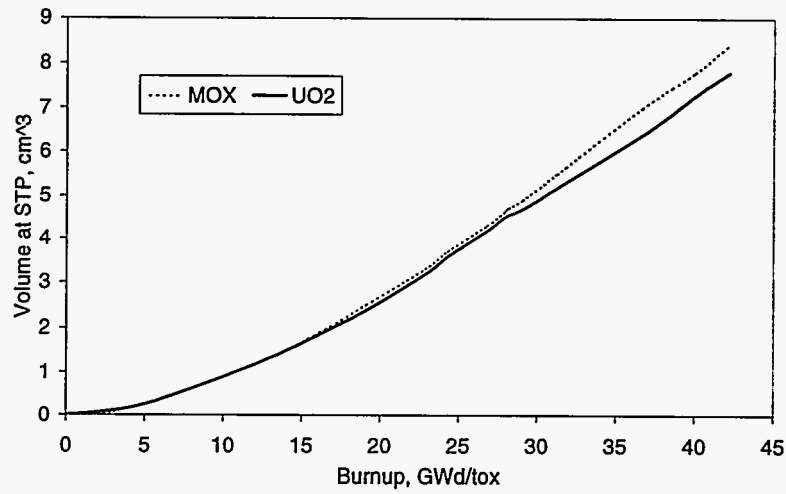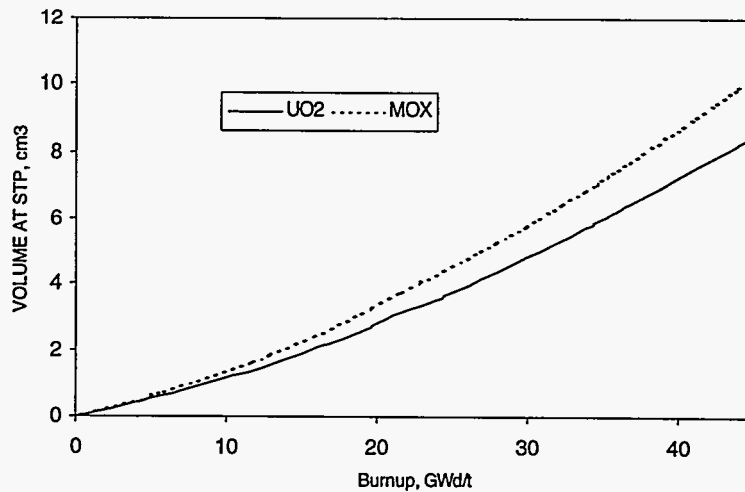
(a) PWR

(b) BWR

(c) WWER

Figure 18: Xe Release to the Free Volume of the Fuel Pin
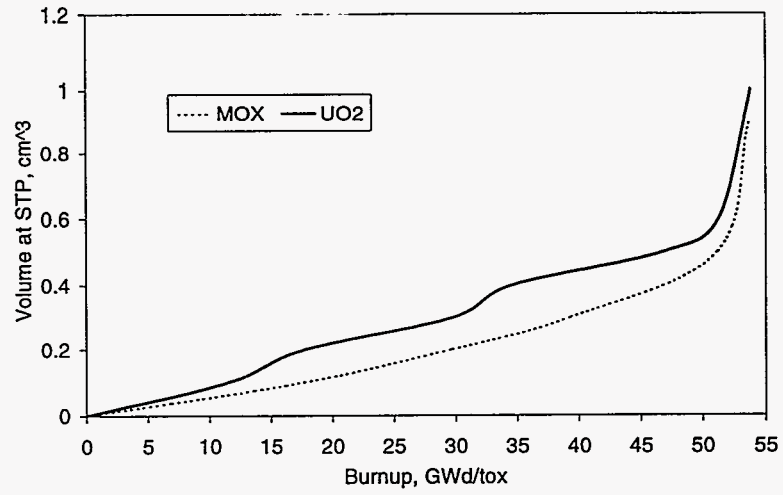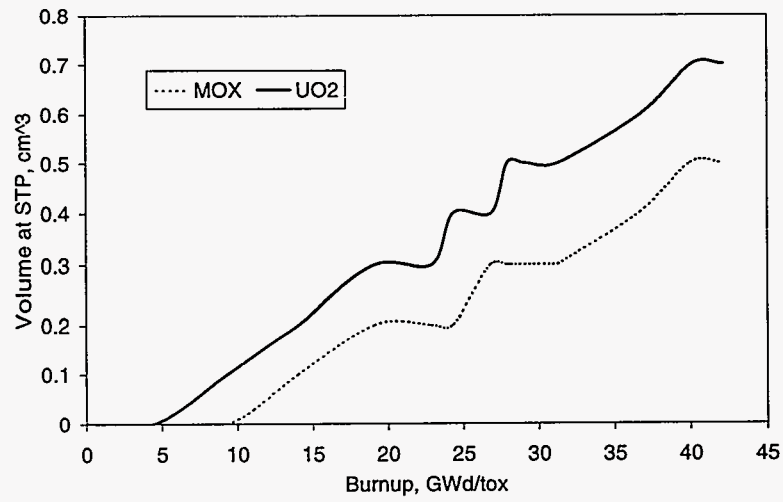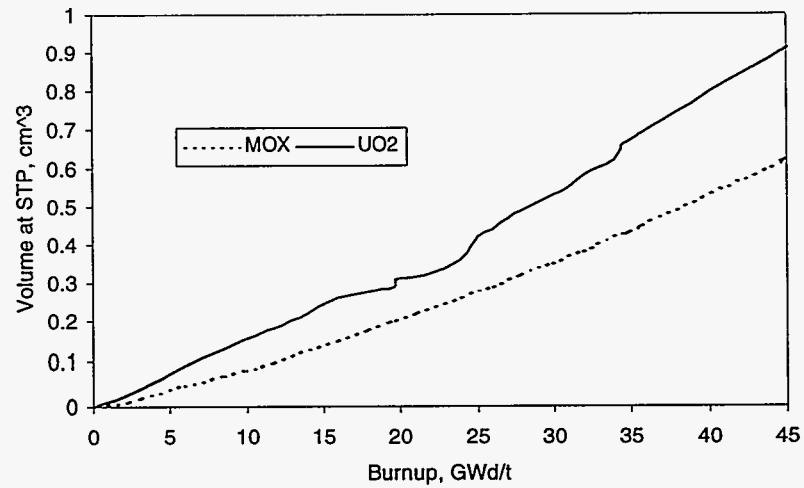
(a) PWR

(b) BWR

(c) WWER

Figure 19: Kr Release to the Free Volume of the Fuel Pin
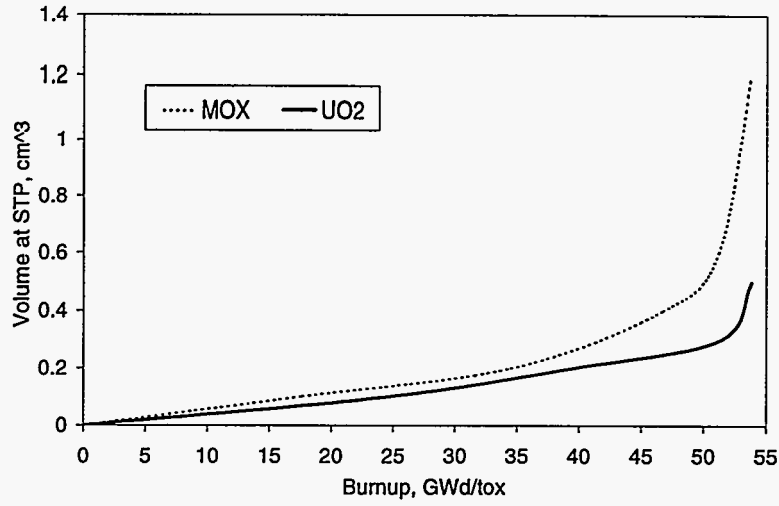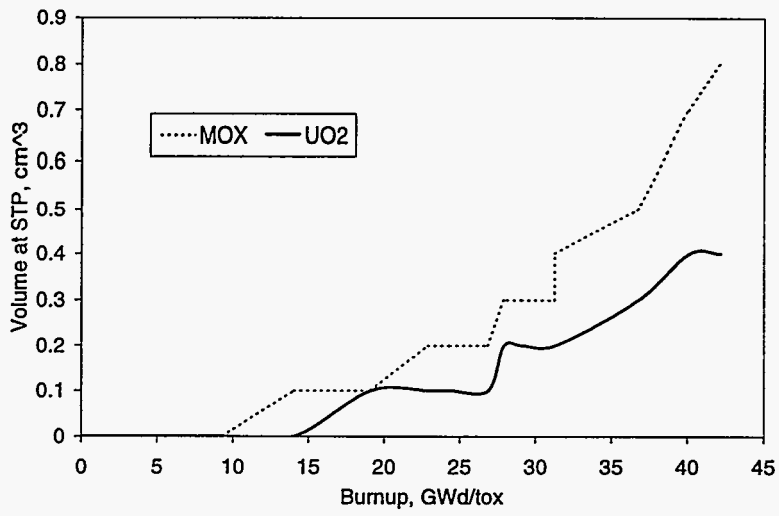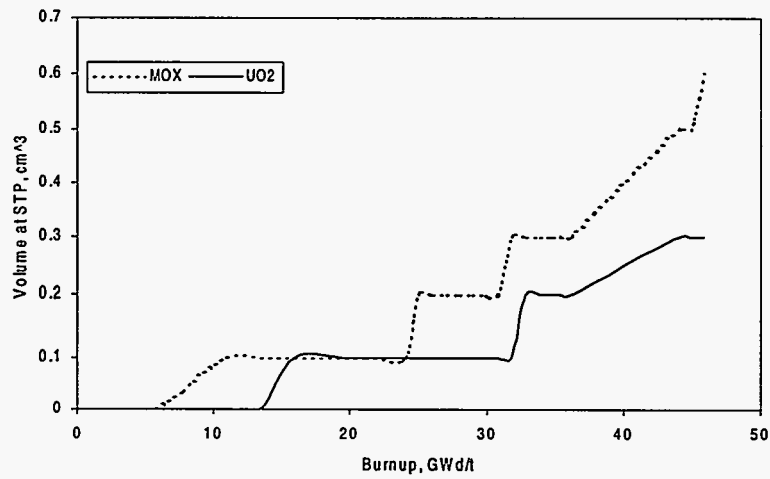
(a) PWR

(b) BWR

(c) WWER

Figure 20: He Release to the Free Volume of the Fuel Pin

41
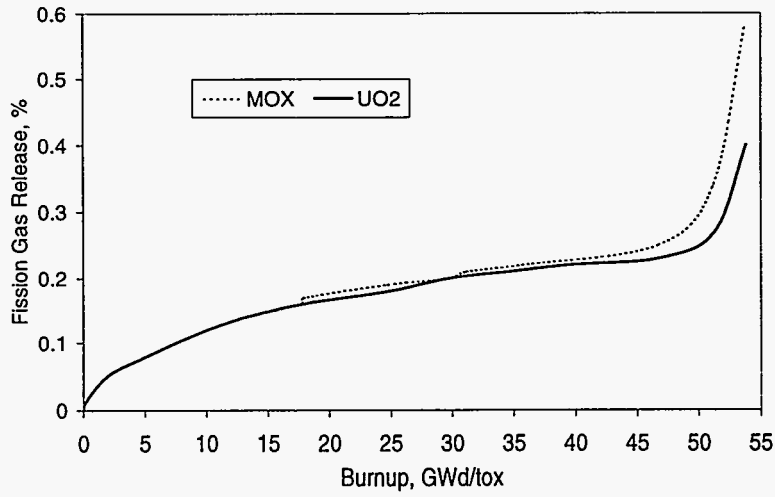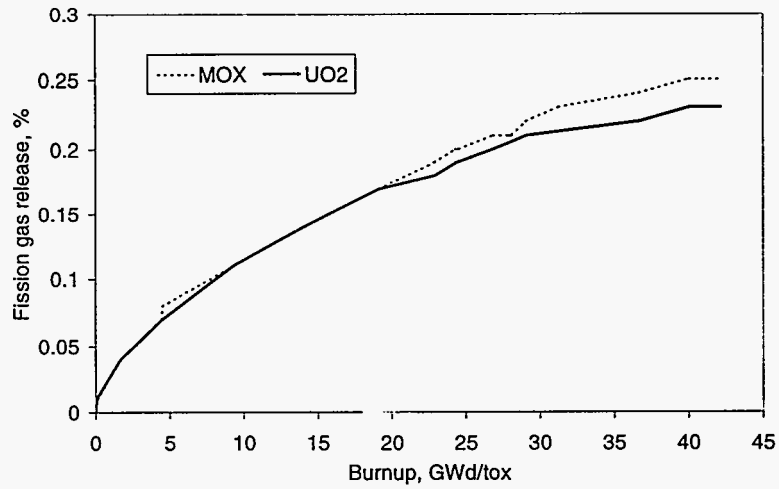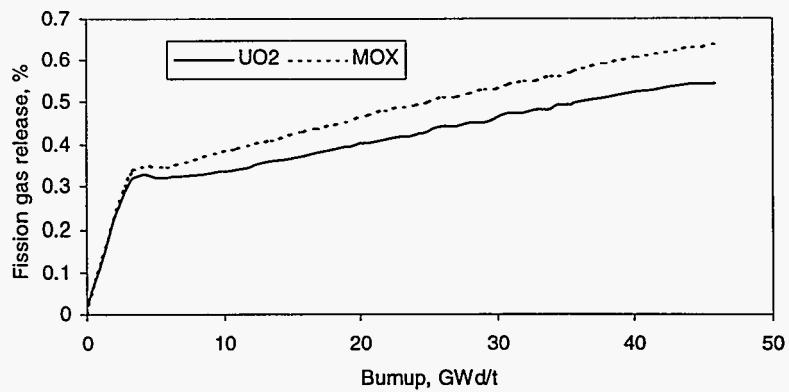
(a) PWR

(b) BWR

(c) WWER

Figure 21: Fission Gas Release

(a) PWR
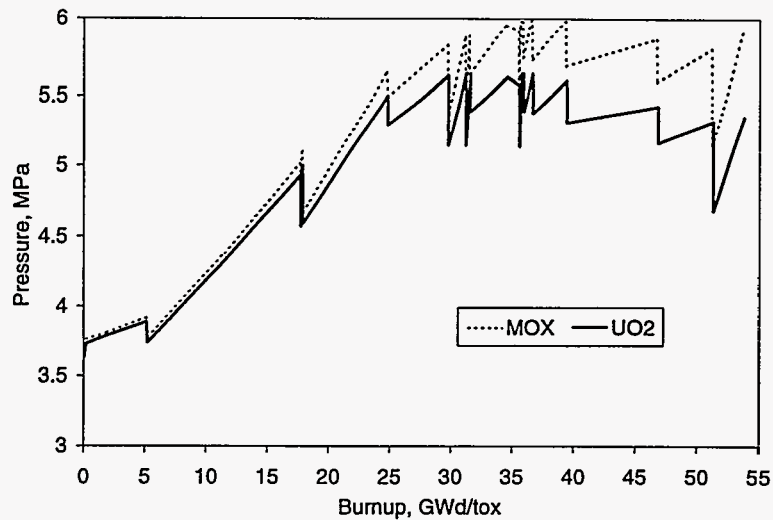
(b) BWR
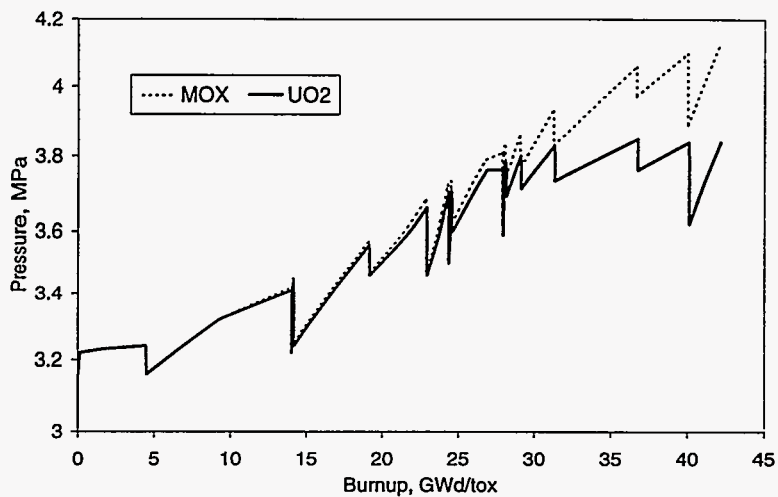
(c) WWER
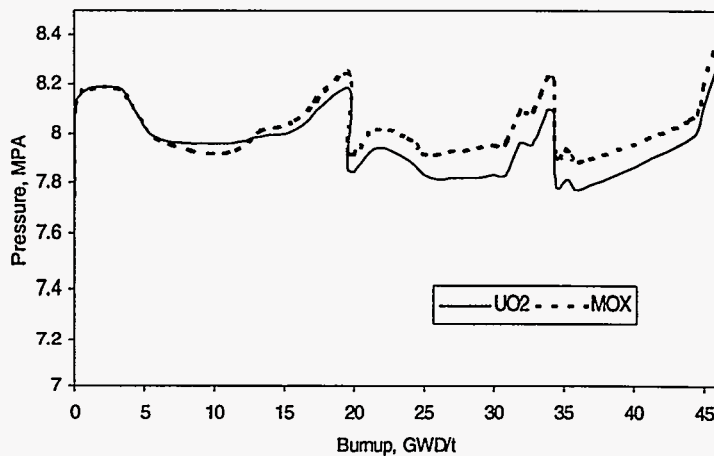
Figure 22: Fuel Pin Inner Pressure at the Hot State

43
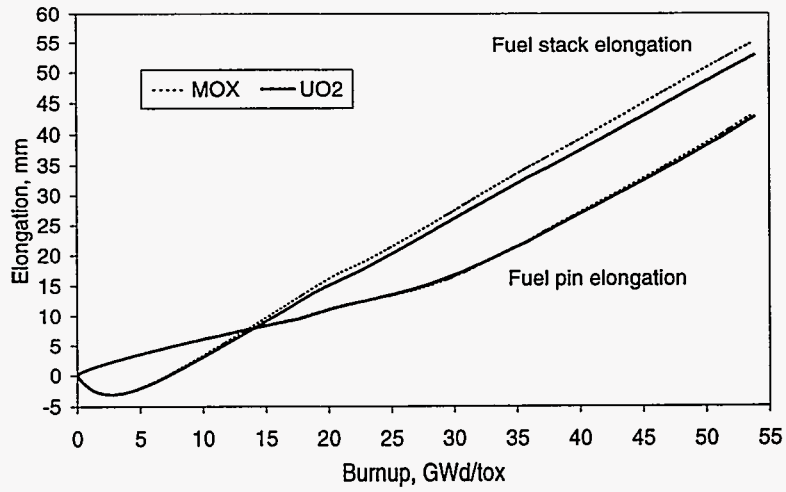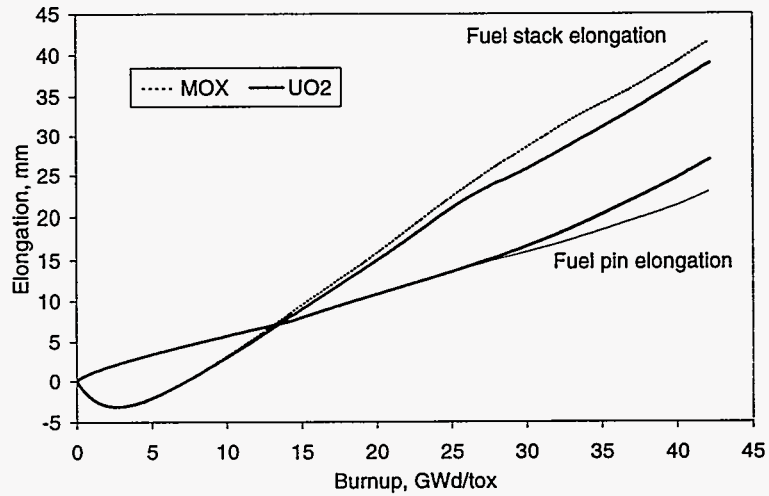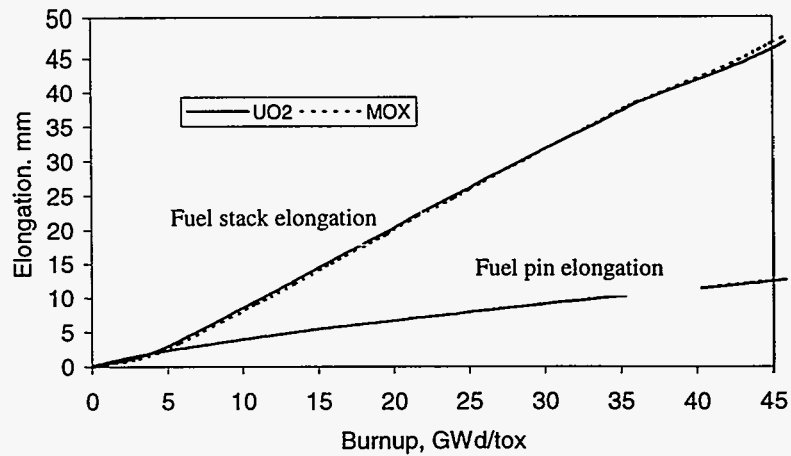
(a) PWR

(b) BWR

(c) WWER

Figure 23: Fuel Pin and Fuel Stack Elongation

44
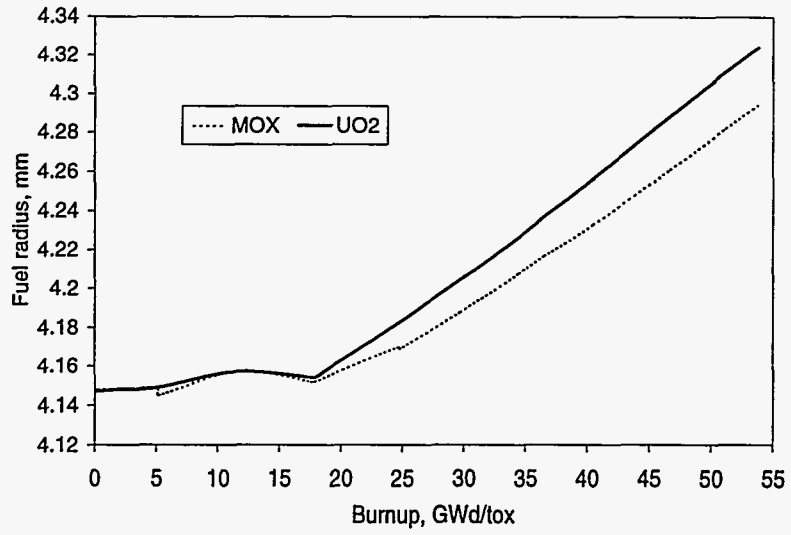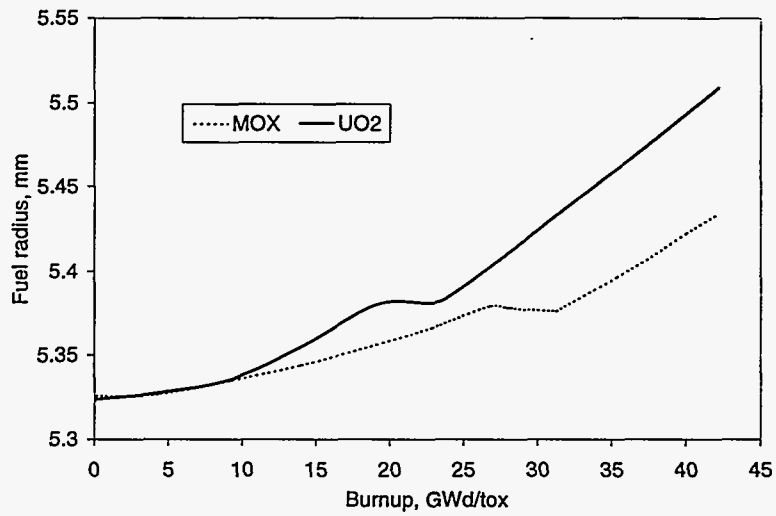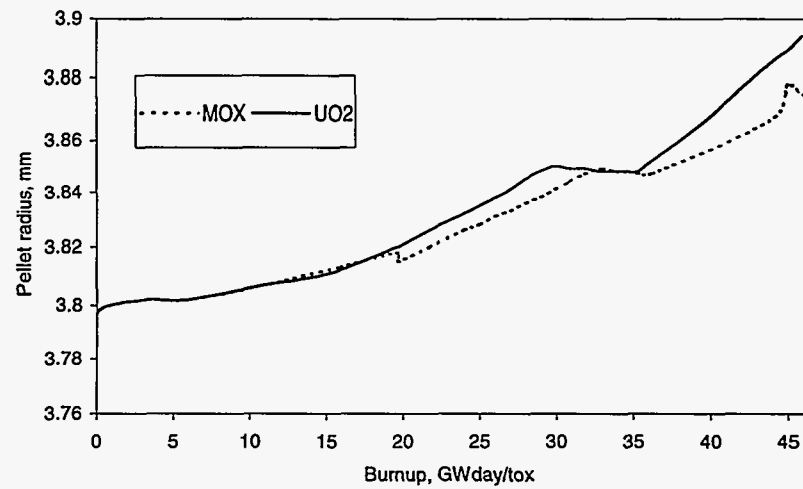
(a) PWR

(b) BWR

(c) WWER

Figure 24: Radial Fuel Growth

45
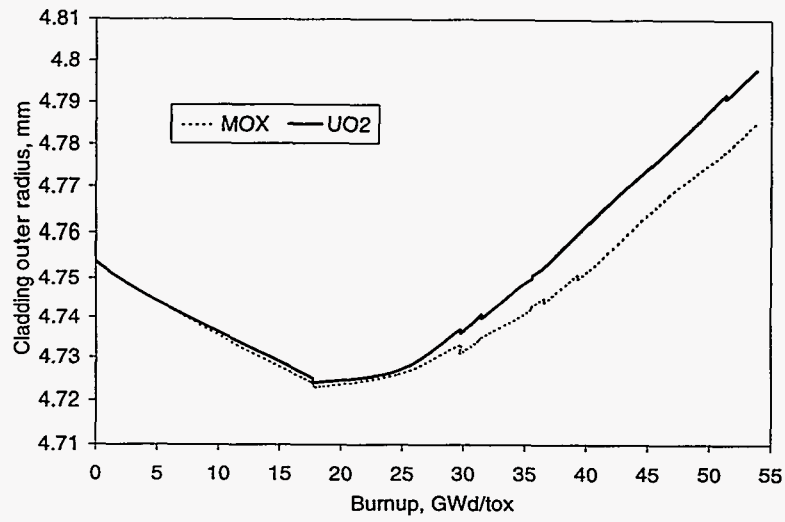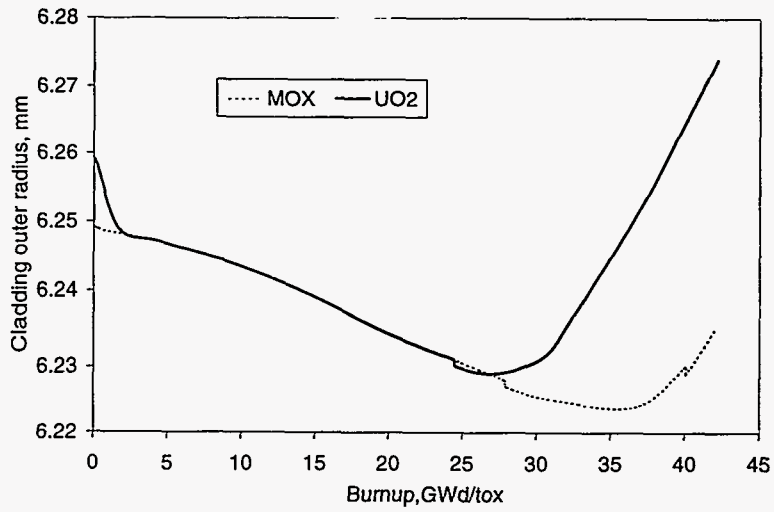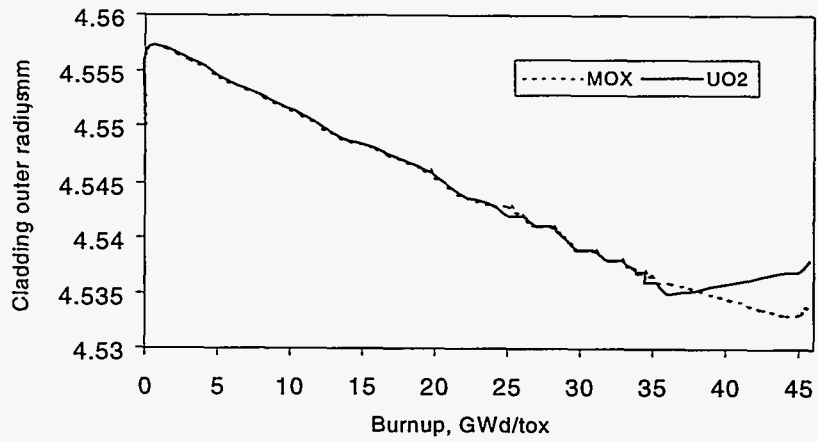
(a) PWR

(b) BWR

(c) WWER

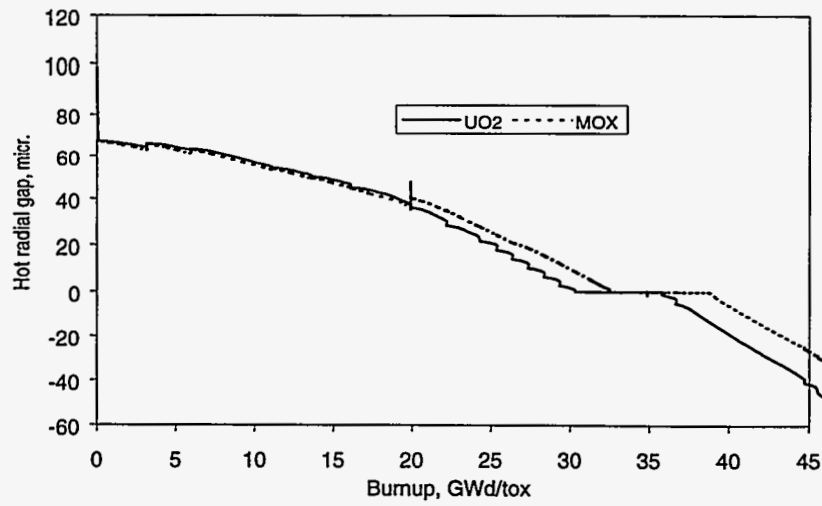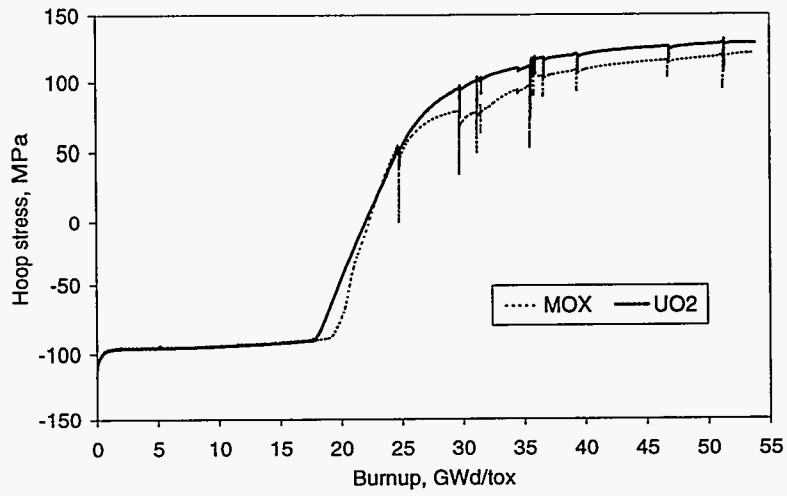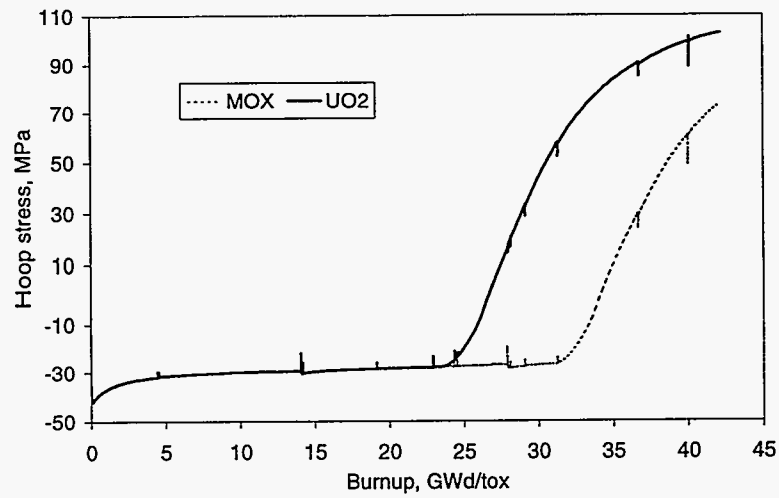**Figure 25**: Change of the Clad Outer Radius with Burn-up

(a) PWR
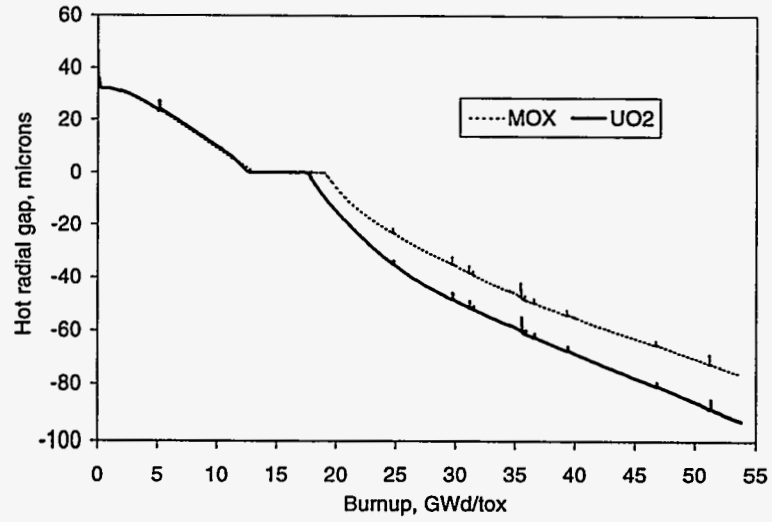
(b) BWR
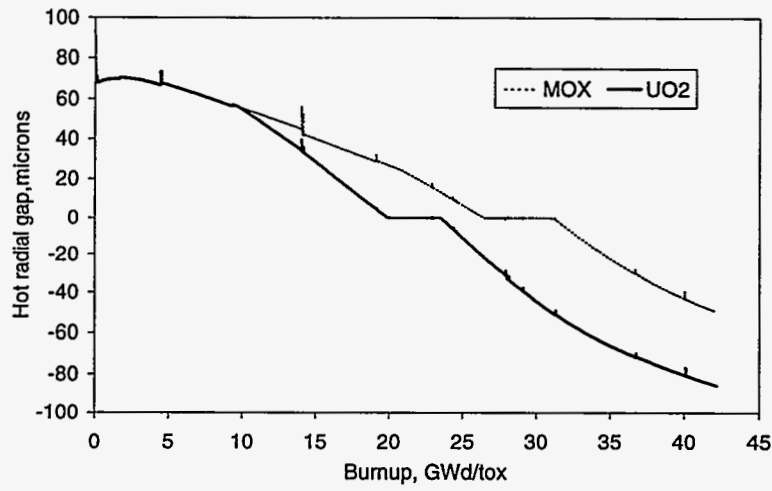
(c) WWER

Figure 26: Dynamics of Pellet-Clad Gap

47
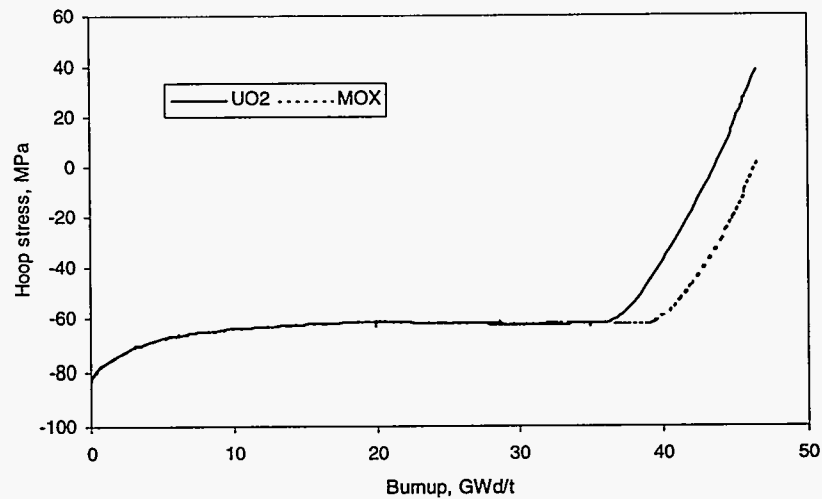
(a) PWR

(b) BWR

(c) WWER

Figure 27: Hoop Stress in the Cladding

48
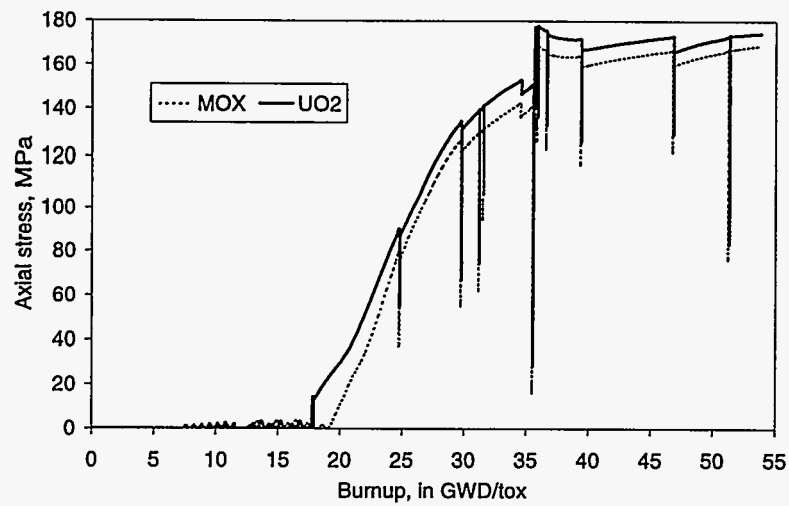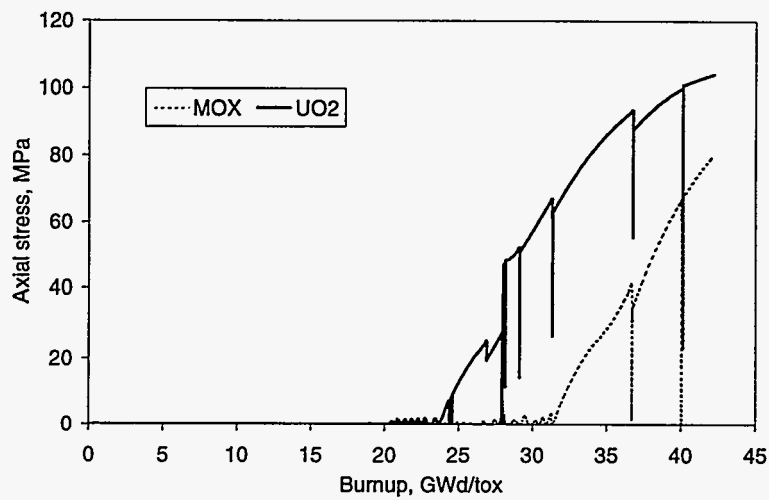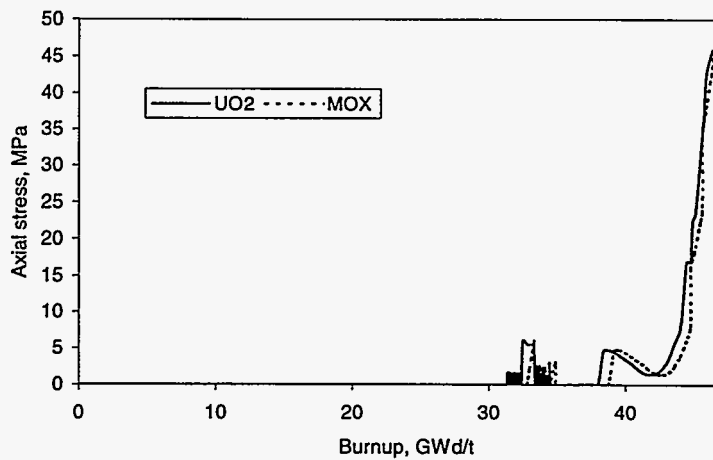
(a) PWR

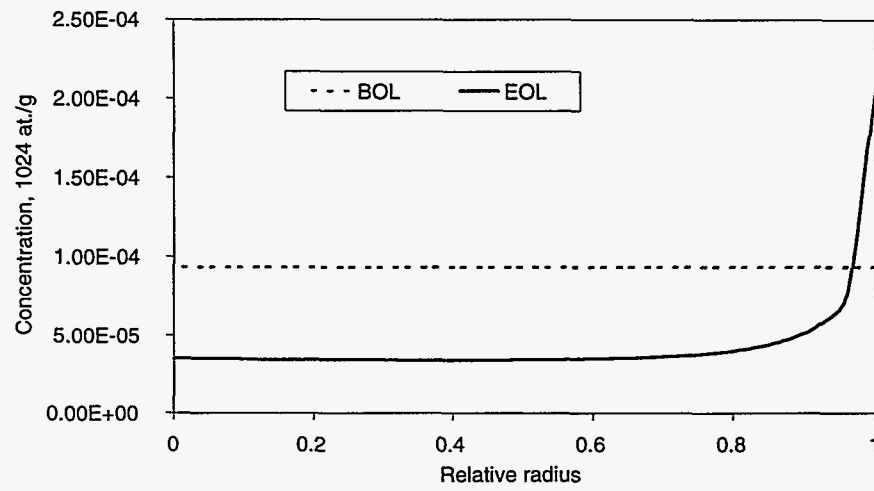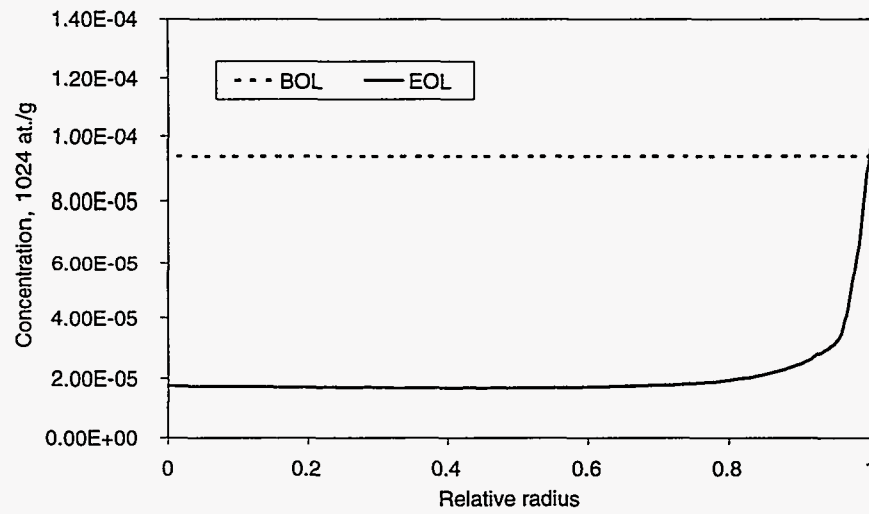
(b) BWR

(c) WWER

Figure 28: Axial Stress in the Clad

49

(a) PWR

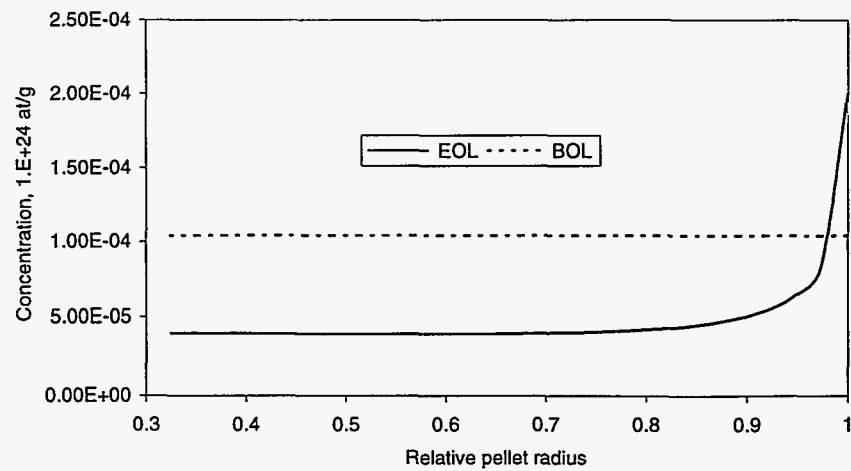

(b) BWR

(c) WWER

Figure 29: Radial Distribution of Pu-239 in MOX Fuel Pellets

REFERENCES

1. Blanpain, P., et al., "MOX Fuel Experience in French Power Plants," Proceedings of the ANS International Topical Meeting on LWR Fuel Performance, West Palm Beach, FL, American Nuclear Society, Inc., La Grange Park, IL, pp. 718-725, 1994.

2. Caillot, L., et al., "Analytical Measurement of Thermal Behavior of MOX Fuel," Proceedings of the ANS/ENS International Topical Meeting on LWR Fuel Performance, Avignon, France, America Nuclear Society, inc., La Grange Park, IL, pp. 651-661, 1991.

3. Deramaix, P., et al., "MIMAS Fuel Performance in Commercial Reactors," Proceedings of the ANS/ENS International Topical Meeting on LWR Fuel Performance, Avignon, France, American Nuclear Society, Inc., La Grange Park, IL, pp. 94-103, 1991.

4. DOE Record of Decision on the Storage and Disposition of Weapons-usable Fissle Materials, January, 14. 1997.

5. Doi, S. and K. Yamate, "High Burnup MOX Fuel and Fuel Rod Design Improvement," Proceedings of the ANS International Topical Meeting on LWR Fuel Performance, Portland, OR, American Nuclear Society, Inc., La Grange Park, IL, 46-53, 1997.

6. N. Hoppe, et al., COMETHE, Version 4D Release 022 (4.4-0.22), Volume 1, General Description, BN 9409844/220 – A, April 1995.

7. Ibid, p. 26.

8. International Atomic Energy Agency (IAEA), Design and Performance of WWER Fuel, Technical Report Series No. 379, Vienna, 1996, p. 38.

9. IAEA, Technical Report Series No. 379, Vienna, 1996, pp. 4-17.

10. "Irradiation Report," NOK-M109 International Program, M109-95/01, November 1995.

11. Jenssen, H.K., et al., "Non-Destructive Post Irradiation Examination of 4 Rods from IFA-606," FIG 98/14, January 1998.

12. Lunde, K., "International Irradiation Program, Instrument of Four Irradiated Fuel Rods for IFA-606," FIG 96/07, BN.REF. 9603346/221, October 4, 1996.

13. Mertens, L., "Irradiation Analysis Procedure of Measurement Results and Analysis of the Data Collected During the Two Phases of Irradiation in a BWR," FIG 97/10, April 1997.

14. Murogov, V., Second International Policy Forum: Management and Disposition of Nuclear Weapons Materials, Landdowne, VA, March 21-24, 1995.

15. The Nuclear Fuel Cycle: Analysis and Management, Chapter 6, pp. 177-180.

16. Nuclear Power Technology, Volume 1: Reactor Technology Marshall, Oxford, 1983.

17. ORNL Foreign Trip Report, ORNL/FTR-6338.

18. Restani, R., et al., "Destructive Tests, Final Report: Ceramography, EPMA, SIMS and Burnup Analyses on Rods I2 and and D3 (Assembly M109)," FIG 98/15, March 1998.

19. Schleuniger, P., et al., "International Irradiation Program, Post Irradiation Examination on Two MOX Fuel Rods," Final Report on NDT, Puncture and Sample Cutting, FIG 96/09, BN.REF. 9607777/221, September 16, 1996.

20. Shcheglov, A.S.; Proselkov, V.N.; Bibilashvili, Yu. K.: Malanchenko, L.L.; Onufriev, V.D.; Yamnikov, V.S.;

Smirnov, V.P.; Smirnov, A.V., "Thermal Characteristics of a Fuel Element of the 5th VVER-1000 Reactor of the Novovoronezhskaya Nuclear Power Plant," Atomnaya Energiya v 74 n 5 May 1993, P. 450-452.

21. U.S. National Academy of Sciences, Management and Disposition of Excess Weapons Plutonium, October 1994.

22. Van der Heyden, P., "Fuel Rods Fabrication Report," M109 96/03, May 1996.